

AD635249

AD635249

HARDENING MECHANISMS IN A COBALT-BASE SUPERALLOY

CHARLES S. LEE

1966

# HARDENING MECHANISMS IN A COBALT-BASE SUPERALLOY

by

Charles S. Lee

---

A Thesis Submitted to the Faculty of the  
DEPARTMENT OF METALLURGICAL ENGINEERING  
In Partial Fulfillment of the Requirements  
For the Degree of  
MASTER OF SCIENCE  
In the Graduate College  
THE UNIVERSITY OF ARIZONA

1966

|                           |   |
|---------------------------|---|
| ACCESSION FOR             |   |
| QST1                      | WHITE SECTION <input checked="" type="checkbox"/> |
| QSC                       | BLUE SECTION <input checked="" type="checkbox"/>  |
| QUANTIFICATION            | <input type="checkbox"/>                          |
| JUSTIFICATION             |   |
| BY                        |   |
| DISTRIBUTION/AVAILABILITY |   |
| DIST.                     | AVAIL. and or SELL                                |

JUL 18 1966  
RECEIVED  
A

### STATEMENT BY AUTHOR

This thesis has been submitted in partial fulfillment of requirements for an advanced degree at The University of Arizona and is deposited in the University Library to be made available to borrowers under rules of the Library.

Brief quotations from this thesis are allowable without special permission, provided that accurate acknowledgment of source is made. Requests for permission for extended quotation from or reproduction of this manuscript in whole or in part may be granted by the head of the major department or the Dean of the Graduate College when in his judgment the proposed use of the material is in the interests of scholarship. In all other instances, however, permission must be obtained from the author.

SIGNED: Charles R. P.

### APPROVAL BY THESIS DIRECTOR

This thesis has been approved on the date shown below:

D. J. Murphy  
D. J. Murphy  
Professor of  
Metallurgical Engineering

6 May 66  
Date

## ACKNOWLEDGMENTS

The author is gratefully indebted to M. S. Roush, Claude Wheeler and their associates at the AiResearch Div. of the Garrett Corp. who supplied the requirement, the material, and many helpful suggestions for the completion of this investigation.

For his patient tutoring in electron microscopy techniques and operation, the author deeply appreciates the help of Mr. Walter Roser for the success which was obtained in that phase of the investigation.

Finally, the author wishes to express his appreciation to Dr. D. J. Murphy for his overall helpful suggestions in facilitating the completion of this work.



## TABLE OF CONTENTS

|   | Page   |
|---|--------|
| LIST OF ILLUSTRATIONS.....  | vi1    |
| LIST OF TABLES.....   | x      |
| ABSTRACT.....   | xi     |
| <br>I. THEORY OF ALLOY STRENGTHENING.....                                   | <br>1  |
| 1.1 General Remarks.....  | 1      |
| 1.2 Solid-Solution Strengthening.....                                       | 2      |
| 1.2.1 Effect of Solute Atoms on<br>Initiation of Dislocation<br>Motion..... | <br>3  |
| 1.2.2 Effect of Solute Atoms on<br>Moving Dislocations.....                 | 5      |
| 1.3 Precipitation Hardening.....  | 6      |
| 1.3.1 The Precipitation Process..   | 7      |
| 1.3.1.1 Solid Solution<br>and Clustering<br>Phases.....                     | <br>7  |
| 1.3.1.2 Intermediate and<br>Equilibrium<br>Precipitates....                 | 9      |
| 1.3.2 Precipitate-Dislocation<br>Interactions.....                          | 11     |
| 1.3.2.1 Non-intersecting<br>Interactions....                                | 12     |
| 1.3.2.2 Intersecting<br>Interactions....                                    | 13     |
| <br>II. PHYSICAL METALLURGY OF COBALT-BASE<br>SUPERALLOYS.....              | <br>17 |

TABLE OF CONTENTS--Continued

|  | Page |
|--|------|
| 2.1 Basic Alloy Composition.....                           | 17   |
| 2.1.1 Background.....                                      | 17   |
| 2.1.2 Solid-Solution Strengthen-<br>ing.....               | 20   |
| 2.2 Carbide Precipitation Systems.....                     | 21   |
| 2.3 Intermetallic Compound Precipita-<br>tion Systems..... | 25   |
| III. OBJECTIVES.....                                       | 29   |
| IV. EXPERIMENTAL PROCEDURE.....                            | 30   |
| 4.1 Procedural Summary.....                                | 30   |
| 4.2 Preparation and Heat Treatment<br>of Specimens.....    | 30   |
| 4.3 Optical and Electron Microscopy...                     | 32   |
| 4.4 X-ray Diffraction and Fluores-<br>cence.....           | 33   |
| V. RESULTS AND DISCUSSION.....                             | 36   |
| 5.1 Heat Treatment Phase.....                              | 36   |
| 5.2 Microscopy Phase.....                                  | 39   |
| 5.2.1 Optical Microscopy.....                              | 39   |
| 5.2.2 Electron Microscopy.....                             | 43   |
| 5.3 X-ray Phase.....                                       | 44   |
| 5.4 Suggestions For Further Work.....                      | 48   |
| VI. CONCLUSIONS.....                                       | 49   |
| REFERENCES.....  | 50   |

TABLE OF CONTENTS--Continued

|   | Page |
|---|------|
| APPENDIX A Hardness and X-ray Data (Table I through V).....     | 53   |
| APPENDIX B Heat-Treatment Curves (Fig. 1 through Fig. 8).....   | 59   |
| APPENDIX C Optical and Electron Microscopy Procedures.....      | 68   |
| APPENDIX D Microscopy Photographs (Fig. 9 through Fig. 48)..... | 72   |

## LIST OF ILLUSTRATIONS

| Figure |  | Page |
|--------|--|------|
| 1.     | Hardness Versus Solution Heat Treat<br>Temperature.....  | 60   |
| 2.     | Hardness Versus Aging Temperature for AR-213<br>Solution Treated at 1800° F for 8 hours....              | 61   |
| 3.     | Hardness Versus Aging Temperature for AR-213<br>Solution Treated at 1900° F for 8 hours....              | 62   |
| 4.     | Hardness Versus Aging Temperature for AR-213<br>Solution Treated at 2000° F for 8 hours....              | 63   |
| 5.     | Hardness Versus Aging Temperature for AR-213<br>Solution Treated at 2100° F for 8 hours....              | 64   |
| 6.     | Hardness Versus Aging Temperature for AR-213<br>Solution Treated at 2200° F for 8 hours....              | 65   |
| 7.     | Hardness Versus Aging Temperature for AR-213<br>Solution Treated at 2250° F for 8 hours....              | 66   |
| 8.     | Hardness Versus Aging Time and Temperature<br>for AR-213 Solution Treated at 2200° F<br>for 8 hours..... | 67   |
| 9.     | AR-213 Aged at 1200° F (unetched) - 700 X....  | 74   |
| 10.    | AR-213 Aged at 1800° F (unetched) - 700 X....  | 74   |
| 11.    | As-Cast AR-213 - 100 X.....  | 75   |
| 12.    | As-Cast AR-213 - 700 X.....  | 75   |
| 13.    | Solution-Treated AR-213 - 100 X.....   | 76   |
| 14.    | Solution-Treated AR-213 - 700 X.....   | 76   |

LIST OF ILLUSTRATIONS--Continued

| Figure |  | Page |
|--------|--|------|
| 15.    | AR-213 Aged at 1200° F - 100 X.....                      | 77   |
| 16.    | AR-213 Aged at 1200° F - 700 X.....                      | 77   |
| 17.    | AR-213 Aged at 1400° F - 100 X.....                      | 78   |
| 18.    | AR-213 Aged at 1400° F - 700 X.....                      | 78   |
| 19.    | AR-213 Aged at 1600° F - 100 X.....                      | 79   |
| 20.    | AR-213 Aged at 1600° F - 700 X.....                      | 79   |
| 21.    | AR-213 Aged at 1700° F - 100 X.....                      | 80   |
| 22.    | AR-213 Aged at 1700° F - 700 X.....                      | 80   |
| 23.    | AR-213 Aged at 1800° F - 100 X.....                      | 81   |
| 24.    | AR-213 Aged at 1800° F - 700 X.....                      | 81   |
| 25.    | AR-213 Aged at 1900° F - 100 X.....                      | 82   |
| 26.    | AR-213 Aged at 1900° F - 700 X.....                      | 82   |
| 27.    | Solution-Treated AR-213 - Carbide Stringer...            | 83   |
| 28.    | As-Cast AR-213 - General Matrix.....                     | 84   |
| 29.    | As-Cast AR-213 - Primary CoAl in Matrix.....             | 85   |
| 30.    | As-Cast AR-213 - Matrix, CoAl and Carboni-<br>tride..... | 86   |
| 31.    | Solution-Treated AR-213 - General Matrix.....            | 87   |
| 32.    | Solution-Treated AR-213 - General Matrix.....            | 88   |
| 33.    | Solution-Treated AR-213 - General Matrix.....            | 89   |
| 34.    | AR-213 Aged at 1200° F - General Matrix.....             | 90   |
| 35.    | AR-213 Aged at 1200° F - Primary CoAl in<br>Matrix.....  | 91   |

LIST OF ILLUSTRATIONS--Continued

| Figure |   | Page |
|--------|---|------|
| 36.    | AR-213 Aged at 1400° F - Primary CoAl.....                  | 92   |
| 37.    | AR-213 Aged at 1400° F - Primary CoAl.....                  | 93   |
| 38.    | AR-213 Aged at 1400° F - Primary and<br>Secondary CoAl..... | 94   |
| 39.    | AR-213 Aged at 1400° F - Primary CoAl.....                  | 95   |
| 40.    | AR-213 Aged at 1600° F - Primary and<br>Secondary CoAl..... | 96   |
| 41.    | AR-213 Aged at 1600° F - Carbonitride in<br>Matrix.....     | 97   |
| 42.    | AR-213 Aged at 1700° F - General Matrix.....                | 98   |
| 43.    | AR-213 Aged at 1700° F - General Matrix.....                | 99   |
| 44.    | AR-213 Aged at 1700° F - CoAl Decomposition..               | 100  |
| 45.    | AR-213 Aged at 1800° F - General Matrix.....                | 101  |
| 46.    | AR-213 Aged at 1800° F - CoAl Decomposition..               | 102  |
| 47.    | AR-213 Aged at 1900° F - General Matrix.....                | 103  |
| 48.    | AR-213 Aged at 1900° F - CoAl Decomposition..               | 104  |

# LIST OF TABLES

| Table |  | Page |
|-------|--|------|
| I     | Heats of Formation and Melting Points for Carbides and Nitrides..... | 54   |
| II    | Hardness of Solution-Treated AR-213 Alloy....                        | 55   |
| III   | Hardness of Aged AR-213 Alloy ( $R_C$ ).....                         | 56   |
| IV    | X-ray Diffraction Data for Extracted Particles.....                  | 57   |
| V     | X-ray Fluorescent Analysis of Extracted Particles.....               | 58   |

## ABSTRACT

A study was made of the heat treatment response and hardening mechanism of an experimental cobalt-base superalloy, AR-213. Solution treatment temperatures in the range of 1800° to 2250° F and aging temperatures from 1200° to 1900° F were investigated. Selected aged specimens corresponding to the 2200° F solution treatment were intensively studied using optical and electron microscopy and x-ray techniques to determine the hardening mechanism.

The results of the study show that a maximum aged hardness of  $R_C$  47 is obtainable. The hardening mechanism is the precipitation of CoAl from the supersaturated matrix at temperatures between 1400° and 1600° F. This precipitate overages relatively rapidly at temperatures above 1600° F. A tantalum-zirconium carbonitride was also present in the alloy in a surprisingly large amount.



## I. THEORY OF ALLOY STRENGTHENING

### 1.1 General Remarks

Except for specialty applications requiring a particular property of a metal, very little use is made of pure metals in structural or load carrying materials. However, if it were possible to obtain pure metals having shear strengths approaching the theoretical minimum of  $G/30$ , where  $G$  is the shear modulus, then it would be possible to select pure metals for these applications on the basis of their melting point or some other parameter. The whole basis of the need for alloy strengthening is that, with the exception of whiskers in the form of perfect single crystals, the theoretical strength limit is not even closely approached in pure metals.

It has been established quite conclusively that the prime reason for the large discrepancy between the theoretical and actual strength of a metal is the existence of dislocations. Since slip, or yielding, results from the movement of dislocations through the crystal lattice to the surface, two approaches are available for strengthening a metal. The first is to

obtain a metal with no dislocations. Unfortunately, except for the aforementioned metal whiskers, metals in such form are not available in practical quantities. A second approach is to hinder or halt the motion of dislocations in the lattice. This latter effect can be accomplished by alloying the pure metal.

The process of alloying can impede dislocation movement by many different methods, but the most common are phase transformation hardening, order-disorder hardening, dispersed-phase hardening, solid-solution hardening and precipitation hardening. Subsequent discussion will be concerned with the latter two methods which are most applicable for superalloys.

## 1.2 Solid-Solution Strengthening

Solid-solution strengthening is brought about by those solute atoms which are present in the matrix of superalloys but not combined as carbides or inter-metallic compounds. The effect of solute atom strengthening in a single phase material has long been observed and utilized, but it was not until dislocation theory was introduced and developed that the actual reasons for the strengthening could be explained. Solute atoms affect the strength of a metal by two general types

of interactions with dislocations. These interactions can be broadly classed as those which impede the onset of dislocation movement and those which impede the moving dislocations themselves.

#### 1.2.1 Effect of Solute Atoms on Initiation of Dislocation Motion

The interaction here is between the "atmospheres" of solute atoms and the grown-in Frank network dislocations. Only a fraction of these dislocations lie in slip planes and are orientated for glide; however, the fact that these pinned portions do lie in slip planes makes them available to act as Frank-Read sources for dislocation multiplication. Cottrell (1953) has shown how the stresses around a dislocation can be relieved by a suitable arrangement of the nearby solute atoms. Fleischer (1964) considers two separate types of interactions between dislocations and solute atoms in metals. These are elastic and chemical.

The elastic interactions arise because the substitutional solute atoms, due either to a size difference or a modulus difference, cause a symmetrical lattice distortion in the matrix. Interstitial solute atoms also cause a distortion, but one which is unsymmetrical. When considering substitutional atom atmospheres, several

possibilities arise, depending on whether or not the substituted atoms are larger or smaller than the matrix atoms. Oversized substitutional solute atoms will be attracted to the tension side of a positive edge dislocation while undersized ones will tend to the compression side. Likewise, interstitial atoms will migrate toward the tension side and vacancies toward the compression side. The effect of such behavior is to increase the stress needed to move the dislocation away from the "atmosphere".

Chemical interactions arise from the migration of solute atoms to the stacking fault region between separated partial dislocations. This migration results in a lowering of the energy of the system in the region between the partials. Subsequent displacing of the partial dislocations away from this region of lower energy necessitates an increased stress. This result is the so-called Suzuki hardening.

The effect of either chemical or elastic interactions of "atmospheres" with grown-in dislocations is, then, to increase the stress required to initiate movement of those portions which happen to lie in slip planes.

### 1.2.2 Effect of Solute Atoms on Moving Dislocations

The preceding section considered the stresses which initiate dislocation motion and which lead to the yield point phenomenon. However, once such dislocations have broken free of their binding atmospheres, whether by applied stress or an increase in temperature, the stress required to keep them in motion decreases. The primary effects of solute atoms upon moving dislocations thus occur through solute atom-dislocation interaction and the dragging of the atmospheres previously discussed. The elastic strains developed by substitutional solute atoms are not comparable to those of precipitates in precipitation hardened systems. Also, particle spacing is too small for optimum hardening. The hardening due to atmosphere dragging can occur only at such combinations of stress and temperature which permit solute atoms to diffuse at the same rate as dislocations. The viscous, dragging effect leads to some of the hardening observable under certain high temperature-low stress conditions.

In general, interstitial solute atoms effect a higher degree of hardening than do the substitutional ones; however, of those constituents used in superalloys

for solution strengthening, the substitutional type greatly predominate.

### 1.3 Precipitation Hardening

Both solid-solution strengthening and precipitation hardening effects are utilized in most commercial alloys designed for high temperature service. Thermal activation, however, is much more effective in allowing dislocations to bypass solute atoms than to bypass larger precipitates or clusters of atoms. Thus, the relative effectiveness of precipitation hardening is greater at higher temperatures than is solid-solution strengthening. Fritzlen et al. (1959) have discussed the practical applications of precipitation hardening to cobalt-base alloys, but a more thorough discussion of the theoretical aspects of this hardening mechanism is pertinent at this point.

Several excellent reviews on the subject of precipitation hardening are available in the literature (Kelly and Nicholson, 1963; Hardy and Heal, 1954). Each contains extensive data on aluminum binaries and similar systems, but almost no discussion of complex alloys such as are utilized for high temperature applications. A study of the simple systems, however, yields the

principles upon which all such precipitation-hardened alloys depend.

### 1.3.1 Precipitation Process

Thomas (1963) proposed the following model to explain the various aspects of the precipitation process.

Solid Solution

Quench; supersaturated solid solution

Excess vacancies → Loops/helices/stacking faults

+

Solute atoms → Clusters → Zones

Intermediate precipitates

Equilibrium precipitates

#### 1.3.1.1 Solid Solution and Clustering Phases

The ability to achieve precipitation hardening depends upon being able to obtain a supersaturated

solid solution. This state depends upon a decreasing solubility of one phase in another with decreasing temperature. A knowledge of the phase diagram is therefore essential or highly desirable. The supersaturated solid solution is generally obtained by quenching the alloy from the single phase terminal solid solution so that a metastable condition is achieved. At the same time, quenching gives rise to a non-equilibrium number of vacancies. These excess vacancies have been observed to precipitate into loops or onto dislocations. In other cases (apparently), they are not precipitated, but are held in solution, probably as a result of interaction with excess solute atoms (Thomas, 1959). Where there are no excess vacancies present, the growth of any clusters (segregation of solute atoms) will practically stop. Thus, at least in aluminum alloys, the formation of dislocation loops in dilute alloys and the condensation of vacancies at dislocations in concentrated alloys must be accompanied simultaneously by solute clustering. The rate of clustering depends upon the quenching temperature and the alloy concentration.

This reaction of solute atoms and vacancies leads to the formation of clusters. These clusters have been observed to form during solution treatment,



during quenching and during aging. They are relatively stable and the atoms occupy normal lattice sites, being completely coherent with the matrix. The growth of such clusters results in their detection by x-ray techniques. They are then termed Guinier-Preston (G.P.) zones. As these zones grow they may undergo internal ordering and may or may not have lattice types that are different from the matrix.

#### 1.3.1.2 Intermediate and Equilibrium Precipitates

The next stage in the process is the formation of intermediate precipitates. These may be partially or wholly coherent, depending on the system, but their presence is usually associated with the peak hardness. The degree of coherency is quite critical to the amount of hardening obtained since it determines the strain energy in the matrix. In fact, peak hardness is presumed to result from overlapping coherency strain fields. Continued growth of the coherent precipitate may raise interfacial shear stresses to a value too high to be sustained and the precipitate then becomes incoherent. Friedel (1964) considers that non-coherency occurs when the precipitate becomes so large that the elastic energy due to the difference

in atomic volume of matrix and precipitate becomes greater than the surface energy.

A list of precipitate shapes and habit planes has been tabulated by Kelly and Nicholson (1963). The most common are spheres, discs, rods or needles, cubes and plates. Of these, the disc is a minimum energy shape for a highly strained precipitate and is the most common shape for intermediate precipitates. In fact, the reason that metastable precipitates form in preference to stable ones is that for stable precipitates, a large surface energy exists between the stable phase and the matrix, whereas for G.P. zones and certain intermediate phases, this surface energy is small since the zone is strictly just a perturbation of the matrix (Fine, 1964). Kelly and Nicholson (1963) also emphasized that there is often little to distinguish the G.P. zones from intermediate phases and they concluded that the term G.P. zone is most useful in describing the initial precipitate where the structure of the precipitate is similar to that of the matrix. The majority of alloys show transition precipitates, but the exact reasons for their existence still remain somewhat in doubt and, in fact, some of them are stable only when nucleated on dislocations.

The equilibrium precipitate is that stable structure which the intermediate precipitates finally take as a result of diffusion toward equilibrium conditions. Here again, the degree of coherency depends upon the system. The importance of coherency in all stages of precipitation is that it determines whether a glide dislocation in the matrix has a Burgers vector the same or nearly the same as in the precipitate, or whether it is quite different.

### 1.3.2 Precipitate-Dislocation Interactions

For full comprehension of the hardening process, an understanding of the actual precipitation mechanisms must be accompanied by an understanding of the precipitate-dislocation interactions. All three of the precipitate types -- G.P. zones, metastable precipitates and stable precipitates -- can interact with moving dislocations to give rise to strengthening, though to different extents. For actual slip to occur, a dislocation must either move around the particles or shear through them. The path of lowest energy will be the one followed.

### 1.3.2.1 Non-intersecting Interactions

The dislocation has two ways of moving around a particle. The first is to leave the slip plane either by cross slip for screw dislocations, or climb for edge dislocations, where the temperature is such that climb can occur. The second is by the Orowan mechanism. These non-intersection types of hardening generally occur with non-coherent, nondeformable precipitates having a crystal structure different from that of the matrix. In the Orowan theory (Orowan, 1954) the slip plane containing the hard precipitates is considered as being traversed by a dislocation which is held up by the particles. The dislocation can then bulge between the particles until neighboring bulges meet, fuse together to reform the dislocation line, and continue along the slip plane. The particles are left encircled by a dislocation ring with each following dislocation adding an additional ring. With increasing deformation the number of encircling rings also increases until the rise in shear stress can break down a particle at which time it ceases to function as a slip deterrent for that particular slip plane. The Orowan expression for the yield stress is:

$$\tau = \tau_d + q G \frac{b}{d}$$

where  $\tau_d$  is the dislocation driving stress,  $q$  is a dimensionless parameter approximately equal to one,  $G$  is the shear modulus,  $b$  is the interatomic spacing in the slip direction and  $d$  is the distance between adjacent precipitates. Thus, the overaging phenomenon corresponding to a coagulation of particles and a corresponding increase in  $d$  can be accounted for. This expression does, however, break down at very low values of  $d$  corresponding to the solid-solution hardening situation.

Both of the previous mechanisms, while not involving the intersection of dislocations with precipitates, do involve a lengthening of the dislocation line itself. This process necessitates an energy increase, and the stress required for this has been found to be proportional to  $\frac{Gb}{d}$  as in the Orowan expression.

#### 1.3.2.2 Intersecting Interactions

The shearing of precipitate particles by dislocations becomes more energetically favorable than bypassing them when the particles are weaker, more closely spaced and more coherent with the matrix. Thomas (1963), in a review of transmission electron microscopy

results, observed that dislocations generally cut through coherent and partially coherent precipitates but they avoided non-coherent precipitates. Fine (1964) listed three basic factors involved in particle cutting: elastic misfit stresses, increase in particle surface area and increase of flow stress necessary to move a dislocation inside the particle.

Elastic misfit stresses arise because the volume occupied by  $N$  atoms in the matrix is, in general, not the same volume as is occupied by  $N$  precipitate atoms. Three separate situations exist for the distribution of a given volume fraction of precipitate. First, the particles can be so small and well distributed that the particle spacing is smaller than the minimum radius of curvature of a dislocation bent under an applied stress. This situation is essentially that which exists for a solid solution, and since the dislocation lies on an equal number of stress "peaks" and stress "valleys", very little strengthening is realized. The second and most important case from the strengthening standpoint is that in which the minimum radius of curvature of a dislocation is approximately equal to the particle spacing. In this instance, the dislocation can take an equilibrium position in the stress "valleys" of elastic misfit and thus

be in its lowest energy configuration. An applied stress, necessary to move this dislocation, will have to force it through the stress "peaks" to affect slip. This is the situation resulting in maximum hardness and is the reason that an optimum dispersion exists for precipitates. The third case is the situation corresponding to overaging. Here the particle spacing is quite large compared with the minimum bend radius of a dislocation. The dislocation is now able to bend between and avoid the second phase, therefore facilitating slip.

The second basic process involved in particle cutting is an increase in surface area of the cut particle. The total energy increase involves the increase in matrix-precipitate interfacial energy plus the chemical energy of misfit due to chemical composition differences across the interface. Also considered is the structural misfit at the interface due to different atomic spacings (Kelly and Nicholson, 1963).

The final process in strengthening by intersected particles is due to the difference in the flow stress for moving a dislocation in the precipitate versus moving it in the matrix. One consideration in

this process is the work done in disordering an ordered precipitate. A second is the work consumed in pulling immobile jogs through the precipitate (the jogs result when the slip planes of matrix and precipitate are not parallel).

The relative effect of each of these sub-mechanisms, naturally, varies with each particular alloy system; however, in general, for thick precipitates, the work done in disordering is predominant.



## II. PHYSICAL METALLURGY OF COBALT-BASE SUPERALLOYS

### 2.1 Basic Alloy Composition

#### 2.1.1 Background

The need for a material for use in turbo-superchargers appears to have provided the real impetus for the development of cobalt-base superalloys. It is a strange fact that Vitallium, an alloy originally developed for dental use, became the first cobalt-base superalloy and was subsequently developed into Haynes-Stellite Alloy No. 21 (HS-21). Years later, the turbo-jet engine extended the requirement for materials with an even higher temperature capability. The list of alloys which has evolved since that time is quite lengthy. Known principally by their trade names due to the lack of any standardization in nomenclature, their compositions and characteristics are not readily apparent. They are best evaluated in terms of the alloying elements they most frequently contain and their high temperature properties. Such properties include, among others, creep-rupture strength, oxidation resistance, thermal shock resistance and metallurgical stability.

The use of cobalt as the basis material rather than simply as an added element is the characteristic which distinguishes the cobalt-base from iron- or nickel-base alloys. In many alloys, however, the basis material constitutes less than 50% of the weight of the alloy so that the distinction is not always obvious. In general, the element of greatest concentration determines the nomenclature. The nominal range of cobalt in cobalt-base alloys varies between 40 and 70 weight percent. The major alloying elements are C, Mn, Si, Cr, Ni, Co, Mo, W, Nb, Ta, Ti, Al, Fe, Zr, and B. The effect of each is not always clear cut, especially when it is present with several other elements in the alloy. In general, however, the elements present in the alloy under study, AR-213, provide the following effects.

Chromium imparts oxidation resistance, as it does in iron- and nickel-base alloys, and contributes to solid-solution strengthening. Aluminum also aids in oxidation resistance and is available to precipitate as an intermetallic. Tungsten and tantalum aid in solid-solution strengthening, and tantalum also forms stable carbide networks and promotes oxidation resistance. Manganese and silicon are de-oxidizers. Zirconium is a scavenger element and also promotes high temperature

strength. The effect of iron, if any, is not clear. The presence of carbon is necessary for the formation of carbides which are a source of strength for practically all cobalt-base alloys.

The amounts of each element must be tailored, within narrow limits, to provide the desired effects. Wheaton (1965) has an excellent discussion on this particular point in a recent paper dealing with the development of a new castable cobalt-base alloy (MAR-M 509). The composition of this alloy was determined by the desire for an attractive combination of properties without emphasizing any single property at the expense of others. In this way, a balance of creep-rupture strength, oxidation resistance, thermal conductivity and stability was obtained.

The amount of carbon in the superalloys demonstrates well the optimization criterion. Carbon concentrations range from approximately 0.07 to 0.9 weight percent. The higher values provide an abundance of carbon for carbide strengthening, but large concentrations of carbides may adversely affect thermal conductivity and promote brittleness. To provide the necessary strength in those alloys with low amounts of carbon it is necessary to add sufficient amounts of refractory

metals and/or elements which can precipitate as inter-metallic compounds.

### 2.1.2 Solid-Solution Strengthening

Some degree of solid-solution strengthening is provided by any element not tied up in secondary phases. In this respect certain elements are much more effective than others. The most effective and widely used are the high-melting refractory metals, tantalum, tungsten, columbium, molybdenum and chromium. In addition to their high melting points, the large atomic size difference of these elements also contributes to the strengthening effect (Nisbet and Hibbard, 1953).

Habraken and Coutsouradis (1965) recently completed a more fundamental investigation of solid-solution strengthening effects in cobalt-base alloys utilizing transmission electron microscopy. In particular, they studied the influence of alloying elements on stacking-fault energies and on the associated partial dislocation separations. Whereas in pure cobalt the stacking-fault energy was approximately  $20 \text{ ergs/cm}^2$ , in a Co-27Cr-20Fe alloy it was about  $5 \text{ ergs/cm}^2$  and the observed partial dislocation separation was greater. A still wider separation was observed in a stronger

Co-20Cr-15W-10Ni alloy. The authors concluded that the Suzuki mechanism was quite important in the hardening of cobalt alloys.

While solid-solution strengthening is a necessary factor in superalloys, no current alloys depend solely upon it for good elevated temperature properties. The most important strengthening mechanism in current alloys is the precipitation of refractory carbides which results from their decreasing solubility with decreasing temperature. Hardening may also be achieved through precipitation of intermetallic compounds; however, this method has not been extensively utilized to date. These hardening mechanisms will now be discussed in detail.

## 2.2 Carbide Precipitation Systems

Carbides are present in superalloys in many distributions and in several crystallographic forms. From the distribution standpoint, it is possible to distinguish between the carbides which form during solidification from the melt and those which are subsequently precipitated during aging treatments. The former include the MC,  $M_6C$ ,  $M_{23}C_6$  and  $Cr_7C_3$ . Those which are usually precipitated are primarily  $M_{23}C_6$  and  $M_6C$ . The effect which any carbide dispersion will have

on strength depends upon the size of the particles and their distribution. Thus, the carbide networks formed during solidification are often not as effective as those formed by subsequent solution treatment and precipitation.

Titanium, zirconium, columbium and tantalum are among the strongest of the MC carbide formers (Wagner and Hall, 1962). These carbides are quite stable, have high melting points, and resist going into solution. In general, where there is an excess amount of the MC carbide-forming element over the amount necessary to tie up all the carbon, the MC carbide will be found almost to the exclusion of the other carbide forms. This was clearly shown in Weeton's and Signorelli's (1955) investigation of S-816 where the high columbium content allowed formation of CbC and effectively suppressed formation of  $\text{Cr}_7\text{C}_3$  and  $\text{M}_6\text{C}$  while greatly limiting the amount of  $\text{M}_{23}\text{C}_6$  present.

The MC carbides are not generally involved in precipitation systems; however, the solubility in cobalt of WC and CbC is 22 and 5 percent respectively, at  $2280^\circ\text{F}$  (Fritzlen, et al., 1959). The possibility exists, then, that these carbides could be precipitated after a solution treatment. However, Lane and Grant (1952), in

an investigation of N-155, which contained three and one-half times as much tungsten as columbium, found no WC but a great deal of CbC and suggested that tungsten does not form its own carbide lattice, but instead, substitutes in the  $M_6C$  and CbC structures. In that same study no  $Mo_2C$  or  $W_2C$  were reported in any of the various cobalt alloys investigated. This account somewhat agrees with the findings of Rosenbaum (1948) who listed various carbide formers in order of decreasing effectiveness - Ti, Cb, W, Mo and Cr. The large amount of chromium in all the above alloys results in this element being a major constituent in  $M_6C$  and  $M_{23}C_6$  even though the more active carbide-forming elements are present. Unfortunately, for comparison purposes, tantalum and zirconium were not present in the alloys investigated by Rosenbaum. These elements rank with titanium as the most powerful carbide formers. An indication of their stability is given by their melting points shown in Table I. The values range from  $7010^{\circ}$  F for TaC down to  $2800^{\circ}$  F for  $M_{23}C_6$ . The relative stability of the MC carbides over the others, however, does not imply that these are stoichiometrically perfect compounds. A good example of this is in Waspalloy in which the primary carbide is not pure TiC, but (Ti,Mo)C (Radavich and

Pennington, 1961). Presumably, this substitution is prevalent in all carbides found in similar alloys.

Tantalum carbide with a maximum solubility of 3 percent in cobalt at  $2280^{\circ}$  F is unlikely to participate in useful precipitation reactions. It is usually found in the as-cast material and its distribution is little changed by solution treatment.

The general trend suggested by the above behavior is that hardening by carbide precipitation usually results from the  $M_{23}C_6$  and  $M_6C$  rather than the MC type. This condition requires a close balance in chemistry between the amounts of carbon and carbide formers. A large excess of the strong carbide formers can tie up all the carbon and prevent its participation in effective precipitation. Fortunately, it appears that, for columbium at least, this element must exist in a quantity appreciably above that theoretically required in order to combine with all the carbon in the alloy (Rosenbaum, 1948). This condition may also apply to tantalum.

Finally, nitrogen in the superalloys acts quite similarly to carbon and its presence can be considered as an increase in the carbon content. In the presence of the strong carbide formers mentioned previously, this



behavior results in the formation of nitrides and carbonitrides, instead of the pure carbides.

### 2.3 Intermetallic Compound Precipitation Systems

Although of academic importance, the use of intermetallic compound precipitation hardening has not been utilized extensively in cobalt-base superalloys. The hardening of these alloys, to date, has relied upon carbide strengthening. This procedure is in contrast to the nickel-base systems in which  $\text{Ni}_3\text{Al}$ ,  $\text{Ni}_3\text{Ti}$ , or  $\text{Ni}_3(\text{Al},\text{Ti})$  are primary hardeners in many alloys.

Fritzlen, et al. (1959) listed aluminum, columbium, tantalum and titanium as elements which can form intermetallic precipitates in cobalt alloys. Tungsten, molybdenum, chromium and vanadium were also listed as possible intermetallic compound formers. Unfortunately, very little work other than investigation of the binary and some ternary alloys of these elements with cobalt has been accomplished. A summary of this information follows.

Tantalum and columbium have quite similar phase diagrams with cobalt (Morral, 1958). These show only a 2 percent decrease in solubility with decreasing temperature. Nevertheless, for dilute alloys of from 3 to

12 percent columbium or tantalum, appreciable hardness increases are found in the 1250 to 1500° F aging temperature range (Fritzlen, et al., 1959). In tantalum, this hardness increase is associated with the precipitation of  $\text{Co}_3\text{Ta}$ , whereas in columbium  $\text{Co}_2\text{Cb}$  is suggested. In commercial alloys neither tantalum nor columbium are available in sufficient amounts to form intermetallics. These elements are tied up as carbides or nitrides or are in solid solution.

Titanium, on the basis of its use in nickel-base alloys, has been considered a prime candidate for hardening in the cobalt systems. The phase diagram shows a decrease in solubility from a maximum of 11 percent at 2080° F to 7 percent at 400° F. Fountain and Forgeng (1959) confirmed the presence of  $\text{Co}_2\text{Ti}$  in aged titanium-cobalt alloys containing 3 to 30 percent titanium. In addition, a new fcc structure was found which has since been identified as  $\text{Co}_3\text{Ti}$ .  $\text{Ti}(\text{C},\text{N})$  phases will form preferentially to the intermetallic compounds, however, and this suggests severe problems in using titanium as an intermetallic precipitate.

The solubilities of molybdenum and tungsten in cobalt are quite extensive. Molybdenum has a solubility of 21 percent at 1860° F which decreases to 2 percent at

400° F, while the solubility of tungsten is 32 percent at 2010° F and decreases to 3 percent at 650° F. Sykes and Graff (1935) obtained a maximum aged hardness of Rockwell C-63 for a cobalt-15 percent molybdenum alloy. The precipitate contained approximately 22 atomic percent molybdenum; however, no crystal structure was determined. Whatever the precipitate, overaging occurred at a relatively low temperature since at 1290° F the maximum hardness had passed after 5 hours.

In the tungsten system, Sykes (1933) found the 15-20 percent tungsten additions most effective on a per atom basis, but obtained a maximum hardness of Rockwell C-65 with a 35 percent tungsten alloy. As to the effect of overaging, the hardness was described as unusually persistent at temperatures as high as 1290° F to 1380° F.

According to the phase diagram, aluminum should be useful as the basis for a precipitant in cobalt. The solubility ranges from 8 percent at 2550° F to almost zero at 200° F. Wheaton (1965) states that although useful as an element to promote oxidation resistance, aluminum has a deleterious effect on creep-rupture strength. However, since AR-213 contains 5 percent aluminum, it will be of interest to consider the intermetallic-compound hardening possible with this element. In alloys containing

up to 34 percent aluminum, the precipitate is CoAl. This phase is bcc having the CsCl structure. The composition of CoAl is quite variable since the phase may contain from approximately 43 to 52 atomic percent cobalt at 400° F. For this reason, its lattice parameter ranges from 2.8505 to 2.8565 Å.

Fritzlen, et al. (1959) show data on the aging behavior of cobalt-aluminum binary alloys containing 4.9 to 15 percent aluminum. The maximum aged hardnesses were obtained by aging at 1110° F for the high aluminum alloys and aging at 1470° F for the low aluminum alloy. Above those temperatures, overaging and a pronounced softening occurred indicating that perhaps CoAl may not be too useful as a hardening agent above 1400° F for a 5 percent aluminum composition. Of course, this behavior of CoAl in the binary alloy can be expected to change somewhat in an alloy of commercial composition. Indeed, all of the data obtained on binaries serve only as a guide toward predicting composition relationships for useful alloys.

### III. OBJECTIVES

The objectives of this investigation of an experimental cobalt-base alloy, AR-213, were essentially threefold and consisted of:

- a. The determination of the heat treatment response of the alloy over a range of solution and aging temperatures and times.
- b. The determination of the actual hardening mechanism in the alloy through study of any observed precipitate dispersion as a function of heat treatment.
- c. The determination, where possible, of the actual composition of the various phases existing in the alloy.

#### IV. EXPERIMENTAL PROCEDURE

##### 4.1 Procedural Summary

The experimental work consisted of three inter-dependent phases. In Phase I, the specimens were prepared from a casting and then solution treated and aged. Hardness readings were obtained for various treatments and then used to select the "optimum" heat treatment. Phase II consisted of an extensive optical and electron microscopy study in which the hardening mechanism was determined. An x-ray evaluation was then undertaken in Phase III to determine the exact nature of the phases present in the alloy.

##### 4.2 Preparation and Heat Treatment of Specimens

The as-cast AR-213 was supplied as cut bars approximately 0.8" x 0.8" x 3" long. These were obtained from the gate of a casting which had been used to furnish multiple cast tensile specimens. The chemical analysis was as follows, in weight percent:

|           |              |
|-----------|--------------|
| Cr - 20.3 | Zr - 0.34    |
| Al - 4.8  | Mn - 0.3     |
| W - 4.5   | Si - 0.28    |
| Ta - 2.3  | C - 0.12     |
| Fe - 0.6  | Co - balance |

A total of 414 specimens approximately 0.4" x 0.4" x 0.25" were prepared from the cast stock, utilizing an alumina cut-off wheel with a high flow of cooling fluid. Great care was exercised in cutting to insure that the specimen temperatures remained as low as possible in order to preclude any extraneous aging effects.

The specimens were then divided into 18 groups, placed in steel boats, and solution heat treated according to the schedule shown in Table II. All heat treating was done in a Despatch tube furnace in air atmosphere. This furnace was capable of holding a 12-inch constant temperature zone and the temperature was readily maintained within  $\pm 7^{\circ}$  F of the desired value. Upon completion of heat treatment, the specimens were removed from the furnace and emptied out in front of a fan for rapid air cooling. Three specimens were then selected at random from each condition and five Rockwell "C" hardness readings were taken on each. The average of

these 15 readings was designated as the solution-treated hardness and is shown in Table II.

Following solution treatment, each specimen was stamped with a letter indicating its particular treatment to preserve its identity through the subsequent aging treatments. The aging cycles comprised an 18 x 24 matrix as shown in Table III. In essence, each solution treatment was represented in one of the 24 different aging conditions. The large number of specimens involved precluded duplicate specimens. Following aging, five hardness readings were taken on each specimen. In all cases the specimen surfaces were hand ground to 600 grit paper smoothness prior to the hardness measurements. The complete hardness results of the aging treatments are shown in Table III and Figs. 1 through 8.

#### 4.3 Optical and Electron Microscopy

Upon completion of the hardness data, the microscopy phase was initiated. Eight specimens were selected from the group which had been solution treated at 2200° F for 8 hours, including the as-cast, the as-cast plus solution treated, and the six aged specimens corresponding to aging at 1200, 1400, 1600, 1700, 1800 and 1900° F



for 32 hours. The basis for selection of this particular set will be discussed later.

The specimens were prepared for microscopy as described in Appendix C. The optical microscopy was done at 100 X and 700 X magnification on a Leitz metallograph. The electron microscopy was performed on an Hitachi HS-7 microscope with the photographs, shown in Figs. 9 through 48, being taken at 5000 X and 10,000 X magnification. The interpretation of these photographs is discussed in the next section.

In conjunction with the microscopy phase, a limited amount of work was done using a microprobe analyzer. From a procedural standpoint, the only variation necessary was to remount the specimens in a conducting resin in place of the lucite mounts.

#### 4.4 X-Ray Diffraction

Attempts were made to identify the various phases in the alloy by means of x-ray diffraction using a General Electric XRD-5 diffraction unit. This investigation took several forms in an attempt to identify all the significant phases. Three techniques were attempted: diffraction from extracted residues, diffraction from powders of the bulk specimens, and

diffraction from the bulk specimens themselves. Chromium radiation was employed in all cases to avoid fluorescence. The extraction technique for carbides was patterned after that of Lane and Grant (1952). This was an electrolytic separation using a pure tantalum cathode with the alloy specimen as anode. The electrolyte was a bath containing equal volumes of:

- a. A solution of 25% phosphoric acid, and
- b. A solution of 25% sulphuric acid with 5% tartaric acid.

An applied voltage of 2 volts and a current of 2 amps was quite sufficient to dissolve the alloy. A magnetic stirrer at the bottom of the cell greatly accelerated decomposition of the specimen so that a time of four hours yielded an abundance of residue. This residue was then agitated in the electrolyte and allowed to set for various time intervals. The relatively large, heavy particles settled rapidly and were left as a residue when the liquid was poured off in one or two minutes. This residue was then placed on a glass slide for x-ray analysis. This procedure simultaneously extracted the precipitated phase and the minor phase in the matrix.

For the powder specimens, filings were ground from the samples and screened to obtain the fraction

less than 300 mesh. This fine powder fraction was vacuum sealed in a pyrex tube and stress relieved at 750° F for one hour. It was then spread on a vaseline coated glass slide for diffraction.

The bulk diffraction specimens simply were ground flat on 600 grit paper and were then ready for analysis.

For fluorescent analysis of the residue, a platinum tube was employed with a LiF crystal. This allowed detection of elements down to chromium.

The x-ray data are tabulated in Appendix E.

## V. RESULTS AND DISCUSSION

### 5.1 Heat Treatment Phase

The work in this phase was directed toward determining an optimum solution treatment for AR-213, and then evaluating the aging responses corresponding to this solution treatment. From an engineering standpoint, however, it was desirable also to determine the heat treatment response of the alloy over a wide range of solution and aging temperatures and times. The purpose of this overall procedure was to detect any incongruous behavior which might occur over the temperature range. The heat treating parameters are shown in Table III. Solution temperatures extended from  $1800^{\circ}$  F to  $2250^{\circ}$  F and aging temperatures from  $1200^{\circ}$  F to  $1900^{\circ}$  F.

It is evident from Table II that solution temperatures below  $2200^{\circ}$  F were, in effect, aging treatments for the as-cast alloy as noted by the hardness increases over that of the as-cast structure. In fact, the as-cast hardness of  $R_C$  25.7 was not quite reached even after 8 hours at this temperature. A marked softening did occur at  $2250^{\circ}$  F; however, at this

temperature molten oxide formed on the surface of the specimens. In addition, danger from incipient melting was present at 2250° F, particularly if any appreciable temperature gradients existed in the furnace. From the practical standpoint, therefore, the 2200° F - 8 hour solution treatment was selected as "optimum" and thus subjected to a more extensive evaluation. It is to be noted, however, that the highest aged hardness obtained in the study,  $R_C$  47.1, was the result of a 1400° F aging of a specimen solution treated at 2250° F. Nevertheless, all work conducted in subsequent phases was given the 2200° F solution treatment.

From the large amount of hardness data tabulated in Table III, only selected portions were plotted in Figs. 1 through 8. The criterion used to fit the curves to the data points was that of obtaining a smooth curve. In several instances this resulted in a curve not passing through a data point. However, since single specimens were used and since composition can vary fairly widely in a casting, it was felt that small hardness differences were not necessarily meaningful.

Figure 1 shows the effect of solution time and temperature upon hardness. There is a consistent, though small, decrease in hardness for longer solution

times. There is no reason to assume that still longer times would not further soften the alloy; however, from the engineering standpoint, such longer times probably would not be practical. Figures 2 through 7 show the effect of aging upon the alloy solution treated at temperatures of  $1800^{\circ}$  to  $2250^{\circ}$  F. Analysis of these curves determined the selection of  $2200^{\circ}$  F as the optimum solution temperature as discussed previously. As can be seen (Figs. 2 through 5), temperatures below  $2200^{\circ}$  served only to age the as-cast structure.

Figure 6 provided the basis for selecting the specimens to be utilized in the microscopy and x-ray portions of the investigation. The six specimens comprising the 32-hour aging curve were those which were subsequently studied in those two phases. Figure 6 shows the expected result, namely, that as the aging time is increased, the peak hardness occurs at a lower and lower temperature. In retrospect, it would have been desirable to have examined the  $1300^{\circ}$  and  $1500^{\circ}$  F aging temperatures to pinpoint the peak hardnesses more accurately.

Figure 8 is simply a cross-plot of Fig. 6, presenting the data in the conventional hardness vs aging time relationship. Several features deserve

comment. The overaging phenomenon observed at 1200<sup>o</sup>, although small, is a real effect. No attempt was made to explore it further since it appeared to have little engineering significance. The 1400<sup>o</sup> curve continues to rise sharply at 32 hours and could be expected to approach the  $R_C$  45-47 range in hardness at some longer time. Aging temperatures of 1600<sup>o</sup> to 1900<sup>o</sup> F all promoted overaging effects prior to 32 hours, with overaging occurring at 1900<sup>o</sup> F in less than 4 hours.

The reasons for the observed responses to heat treatment will be covered next in the discussion of the microscopy phase.

## 5.2 Microscopy Phase

### 5.2.1 Optical Microscopy

The purpose of this phase was to correlate the heat treatment responses with microstructures in order to determine the hardening mechanism in the alloy. In most cases the caption associated with the microstructure of each of the figures from 9 through 48 is sufficient to explain it. First, however, a familiarity with the identity of the phases which appear in the microstructures is necessary. Figures 9 and 10 are good representative structures and can be used to

describe the appearance of the phases observable in the various photomicrographs.

The dark grey phase of Fig. 9 is primary CoAl in a cobalt-rich solid solution. The stringer-like phase is a carbonitride with a probable composition of  $(Ta,Zr)(C,N)$ . Figure 10 shows the only other phase of interest - the general precipitate in the matrix. This phase will be called secondary CoAl so that the two CoAl phases will not be confused. The two triangular inclusions at the upper-center in this picture should also be noted. Lund and Wagner (1962), in a report on constituents in superalloys, reported that nitrides high in carbon often have a black dot in their centers. This photomicrograph supports the premise of a carbonitride in the AR-213 alloy.

The basis for calling the dark phase CoAl is three-fold. First, the cobalt-aluminum phase diagram predicts this phase due to the lack of any appreciable solubility of aluminum in cobalt (see Section 2.3). Secondly, research by W. J. Boesch, unpublished, but reported by Fritzlen, et al. (1959), shows the microstructure of a 92 percent cobalt - 8 percent aluminum alloy which is very similar in many respects to aged AR-213. Finally, x-ray data in the present study



confirms the presence of the CoAl structure. This finding will be discussed in more detail later.

With the above-described phase identifications as a basis, the full set of photomicrographs may now be analyzed. As stated previously, all the microscopy work shown in Figs. 9 through 48 was performed on specimens which were solution treated at  $2200^{\circ}$  F for 32 hours. The sequence of pictures is presented in a definite order to best show the aging characteristics of the alloy. Figures 11 through 26 show the change in structure from the as-cast through the aged condition. Each optical photomicrograph at 100 and 700 X corresponds to a given heat treatment.

The cast structure of AR-213 (Figs. 11 and 12) is typically cored with the primary CoAl being quite angular. A marked increase in homogeneity can be seen in Fig. 13 for the solution treated condition. The carbonitride phase is now clearly accentuated. Some smaller particles of CoAl are now present in the matrix in Fig. 14; however, these are the result of a redistribution, not a precipitation of this phase.

Figures 15 and 16 represent the lowest aging temperature -  $1200^{\circ}$  F. The matrix is still quite clean and, in fact, shows almost no difference from the solution treated condition.

While Fig. 17 shows no change in microstructure due to the higher 1400° F aging, Fig. 18 shows the first indication of the general matrix precipitation which is associated with the maximum hardness for this series. The precipitate is CoAl which is beginning to come out of solid solution.

Figures 19 through 26 show the overaging effects of the higher temperatures. Not only is overaging occurring at these higher temperatures, but in Fig. 22 it can be seen that the primary CoAl is beginning to change morphology. By analogy to the aforementioned work by Boesch, this change is associated with the "precipitation" of cobalt solid solution in the CoAl phase. Figure 26 shows this effect even more clearly, along with denuded zones adjacent to the CoAl.

Finally, Fig. 27 shows a stringer-like phase which was observed in the solution treated condition. A microprobe analysis of this phase showed that it contained a much higher percentage of tantalum than did the adjacent matrix. Its probable composition is, therefore,  $TaC$ . Under the optical microscope, this phase appeared white, whereas the carbonitride previously mentioned had a quite distinctive pink color.

### 5.2.2 Electron Microscopy

The pictures in this series are arranged in the same sequence as were those in the preceding section. No attempt will be made here to discuss each photograph since the captions are self-explanatory. In most cases, correspondence with the associated optical microscopy can readily be made.

In the as-cast structure one point worthy of mention is the high degree of homogeneity of the CoAl phase as seen in Figs. 29 and 30. Figure 30 shows very nicely the typical arrangement of the constituent phases in the alloy. The carbonitride phase at the left generally formed between the matrix and the primary CoAl.

The solution-annealed series (Figs. 31 through 33) all show primary CoAl in a matrix free from general precipitation. No general precipitate is yet visible in Figs. 34 or 35, which were taken of the 1200° F aged specimen; however, in Fig. 35, the first indication is present of the break-up of the CoAl. This trend is even clearer in Figs. 36 through 39 which show "decomposition" of this phase at 1400° F. Figure 38 should be compared with Fig. 18 to get an appreciation of the distribution of the hardening precipitate. A definite

Widmanstätten pattern is evident in the initial precipitation. Unfortunately, no specimens were heat treated between 1200° and 1400° F so that this picture represents the first detection of the particles.

The overaging of the precipitates can be seen in Figs. 42 and 43, showing a specimen aged at 1700° F. Continuous precipitation of CoAl along the same crystallographic planes has formed rod-like particles of the phase, many of which have coalesced. Simultaneous with this precipitate growth is the general break-up of the CoAl phase shown in Fig. 44. This is striking evidence of what Boesch termed "precipitation of solid solution within the CoAl phase".

Figures 45 through 48 show overaging of the precipitates and further break-up of the primary CoAl.

### 5.3 X-Ray Phase

The purpose of this phase of work was to determine the exact nature of the metallographic phases present. From the microscopy work which had just been completed, four such phases needed to be identified.

These were:

- a. The matrix
- b. The primary phase in the matrix

- c. The precipitate in the matrix
- d. The pink inclusions.

The matrix was obviously cobalt solid solution but determination of the other phases required identification by x-ray diffraction. Using procedures described in Section 4.4, a residue of extracted material was obtained and analyzed by diffraction. Typical results are shown in Table IV. Based upon the chemistry of the alloy, TaC and perhaps smaller amounts of  $M_{23}C_6$  or  $M_6C$  were expected. Instead, the prime constituents identified were a face-centered cubic structure having  $a_0 = 4.56 \text{ \AA}$  and a simple cubic structure with  $a_0 = 2.88 \text{ \AA}$ . The first of these corresponded exactly to ZrN (NaCl structure) as seen in Table IV. Matching of the first six lines for this compound verified its presence. Further, since the melting procedure for this alloy involved an air melt, and since ZrN is the most stable nitride formed from the metals present, the procedural history also points to ZrN as the identity of this compound. Remaining to be determined at this stage was the disposition of the carbon in the alloy. Since tantalum was present and is known to be a powerful carbide former, it was expected that the carbon would be found combined in the form of TaC.

Since the diffraction data did not clear up the identification of the hard phase, an x-ray fluorescent analysis was performed on the same extracted particles. The results of this are shown in Table V. As can be seen, the extractions contained a much higher percentage of zirconium and tantalum than did the matrix. It seemed possible, therefore, that the inclusions were a compound based upon Ta, Zr, C and N. The structure and parameters of the possible carbides and nitrides involved are:

|     |     |               |
|-----|-----|---------------|
| TaN | hcp | ----          |
| TaC | fcc | $a_0 = 4.456$ |
| ZrN | fcc | $a_0 = 4.56$  |
| ZrC | fcc | $a_0 = 4.696$ |

Although ZrN and ZrC are known to form a continuous series of solid solutions, TaN and TaC do not form a single stable solid solution (Samsonov and Umanskiy, 1962).

In view of the above information Ta(C,N) does not exist as a single phase. Since, with the exception of a few isolated white carbide stringers, only one hard phase was observed, this single pink phase must contain both the zirconium and tantalum and is presumed to be of the form (Ta,Zr)(C,N).

The only other identifiable x-ray pattern obtained from the residues corresponded to CoAl (Table IV). The identification of this compound became possible only after investigators at AiResearch produced pure CoAl and obtained a diffraction scan from it. The information obtained suggests that the ASTM card file for CoAl is incomplete. The pattern actually obtained for CoAl is of the CsCl type, indicating that the CoAl phase is ordered. This fact is also indicated by the presence of the (100) reflection. Since this compound exists throughout the matrix at all times, its presence as the precipitate phase cannot be directly confirmed by x-ray. However, on the basis of microscopy and because no new phases were present in the x-ray diffraction patterns for the aged alloy, it seems reasonable to conclude that the precipitate observed is CoAl.

The diffraction data obtained from the powdered alloy were of no value in the investigation. The only lines obtained were those presumably associated with the solid-solution matrix phase. Neither the carbonitride nor CoAl peaks were present.

Diffraction from the surface of the bulk specimen was impossible due to the large grain size of the cast material.

#### 5.4 Suggestions for Additional Work

Three prime areas of this investigation warrant further study in more detail.

- a. It is believed that direct aging of the as-cast structure would result in hardnesses comparable to those obtained by solution treating and aging. This could be readily determined.
- b. The longest aging time employed in this work was 32 hours. The phase morphology and stability should be determined after 100 and 1000 hour exposures at temperatures to 1900° F.
- c. The exact nature of CoAl precipitation in a cobalt matrix should be examined, preferably using transmission electron microscopy techniques. This study should concentrate on the 1200° - 1400° F range.



## VI. CONCLUSIONS

1. AR-213 is a precipitation-hardenable cobalt-base superalloy which requires a minimum temperature of  $2200^{\circ}$  F to obtain complete solutioning.

2. The precipitate phase is CoAl which allows for a maximum aged hardness of  $R_C$  47. The CoAl precipitate overages rather rapidly at temperatures above  $1600^{\circ}$  F.

3. An excessive amount of a hard phase identified as (Ta,Zr)(C,N) was present in the alloy indicating that excessive amounts of zirconium and/or nitrogen were present. Other than in isolated stringers, no distinct carbide phase was found.

4. The hardening effect in the alloy was, therefore, associated completely with the precipitation of CoAl.

## REFERENCES

- Cottrell, A. H. (1953), Dislocations and Plastic Flow in Crystals, Oxford Press, London, 134.
- Federighi, T. and Thomas, G. (1962), Phil. Mag., 7, 127.
- Fine, M. (1964), The Strengthening of Metals, Reinhold Publishing Corp., New York, 141-199.
- Fleischer, R. L. (1964), "Solid-Solution Hardening", The Strengthening of Metals, Reinhold Publishing Co., London, 94.
- Fountain, R. W. and Forgeng, W. D. (1959), Trans. AIME, 215, 998.
- Friedel, J. (1964), Dislocations, Addison-Wesley Publishing Co., London, 371.
- Fritzlen, G. A., Faulkner, W. H., Barnett, D. R., and Fountain, R. W. (1959), "Precipitation in Cobalt-Base Alloys", Precipitation From Solid Solution, ASM, Cleveland, Ohio, 449-494.
- Habraken, L. and Coutsouradis, D. (March, 1965), Cobalt, 26, 10.
- Hague, J. R., Lynch, J. F., Rudnick, A., Holden, F. C. and Duckworth, W. H. (1963), Technical Documentary Report No. ASD-TDR-63-4102, Air Force Materials Laboratory, Wright-Patterson AFB, Ohio.
- Hardy, H. K., and Heal, T. H. (1954), Progress in Metal Physics, Vol. 5.
- Kelly, A., and Nicholson, R. B. (1963), Progress in Metal Science, Vol. 10, No. 3.
- Lane, J. R. and Grant, N. J. (1952), Trans. ASM, 44, 113.

- Lund, C. H., and Wagner, H. J. (Nov. 15, 1962), "Identification of Microconstituents in Superalloys", DMIC Memorandum 160, Battelle Memorial Institute, Columbus, Ohio.
- Morral, F. R. (1958), Cobalt and Its Alloys (A Summary of Allotropy and Phase Diagrams), Cobalt Information Center, Columbus, Ohio.
- Metals Reference Book (1962), Vol. II, 3rd Ed., Butterworths, London, 633.
- Nisbet, J. D., and Hibbard, W. R., Jr. (1953), Trans AIME, 197, 1149.
- Orowan, E. (1954), "Dislocations and Mechanical Properties", Dislocations in Metals, AIME, New York, New York, 128-134.
- Radavich, J. F., and Pennington, W. J. (Feb., 1961), Metal Progress, 79, (2), 94.
- Rosenbaum, B. M. (July, 1948), NACA Technical Note No. 1580.
- Samsonov, G. V., and Umanskiy, Ya. S. (June, 1962), "Hard Compounds of Refractory Metals", Technical Translation TT-F-102 NASA.
- Sykes, W. P. (1933), Trans. ASM, 21, 385.
- Sykes, W. P., and Graff, H. F. (1935), Trans. ASM, 23, 249.
- Thomas, G. (1959), Phil. Mag., 4, 606, 1213.
- Thomas, G. (1963), "The Structure of Precipitation-Hardened Alloys", Electron Microscopy and Strength of Crystals, Interscience Publishers, New York, 793-859.
- Wagner, H. J., and Hall, A. M. (July 6, 1962), "Physical Metallurgy of Cobalt-Base Superalloys", DMIC Report No. 171, Battelle Memorial Institute, Columbus, Ohio.

Weeton, J. W., and Signorelli, R. A. (March, 1954),  
NACA Technical Note 3109.

Wheaton, H. L. (Dec., 1965), Cobalt, 29, 163.

APPENDIX A

TABLES

Hardness and X-ray Data

TABLE I

Heats of Formation and Melting Points for  
Carbides and Nitrides

| <u>Compound</u>                                    | <u>M.P. °F<sup>a</sup></u> | <u>-ΔH Kcal/mol<sup>b</sup></u> |
|--|----------------------------|---------------------------------|
| TaC  | 7010 ± 300                 | 38.5                            |
| CbC  | 6330 ± 30                  | 33.7                            |
| ZrC  | 5490 - 6460                | 44.1                            |
| TiC  | 5480 - 5880                | 43.9                            |
| WC   | 4710 - 5220                | 9.1                             |
| Mo <sub>2</sub> C                                  | 4870 ± 40                  | - 4.2                           |
| Cr <sub>3</sub> C <sub>2</sub>                     | 3430                       | 21.0                            |
| Cr <sub>7</sub> C <sub>3</sub>                     | 3150 ± 90                  | 42.5                            |
| Cr <sub>23</sub> C <sub>6</sub> (C <sub>4</sub> C) | 2800 ± 30                  | 16.4                            |
| AlN  | 4050                       | 76.5                            |
| TaN  | 5230 - 5590                | 59.0                            |
| TiN  | 5340 ± 50                  | 80.4                            |
| ZrN  | 5400 ± 50                  | 87.3                            |

a. Hague, et al. (1963)

b. Metals Reference Book (1962)

TABLE II

## Hardness of Solution Treated AR-213 Alloy

| Temperature<br>°F | Time<br>hr. | Hardness<br>R <sub>C</sub> |
|-------------------|-------------|----------------------------|
| 1800              | 2           | 40.5                       |
| 1800              | 4           | 39.7                       |
| 1800              | 8           | 38.9                       |
| 1900              | 2           | 37.6                       |
| 1900              | 4           | 37.5                       |
| 1900              | 8           | 36.9                       |
| 2000              | 2           | 34.4                       |
| 2000              | 4           | 34.0                       |
| 2000              | 8           | 32.1                       |
| 2100              | 2           | 31.2                       |
| 2100              | 4           | 31.3                       |
| 2100              | 8           | 30.6                       |
| 2200              | 2           | 27.1                       |
| 2200              | 4           | 26.1                       |
| 2200              | 8           | 26.3                       |
| 2250              | 2           | 25.2                       |
| 2250              | 4           | 24.5                       |
| 2250              | 8           | 23.2                       |

Note: As-Cast Hardness was 25.7

TABLE III

Hardness of Aged AR-213 Alloy ( $R_C$ )

| Temperature<br>(°F) | Time<br>(hr) | Aging Treatments |      |      |      |       |      |      |      |       |      |      |     |
|---------------------|--------------|------------------|------|------|------|-------|------|------|------|-------|------|------|-----|
|                     |              | 1200°            |      |      |      | 1400° |      |      |      | 1600° |      |      |     |
|                     |              | 4                | 8    | 16   | 32   | 4     | 8    | 16   | 32   | 4     | 8    | 16   | 32  |
| 1800°               | 2            | 39.9             |      | 41.1 | 40.0 | 40.7  |      | 42.0 | 42.8 | 41.1  |      | 42.6 | 41. |
|                     | 4            | 39.4             |      | 39.9 | 40.8 | 39.3  |      | 42.2 | 41.2 | 41.0  |      | 41.6 | 41. |
|                     | 8            | 39.4             |      | 40.7 | 41.2 | 39.5  |      | 41.1 | 42.0 | 41.0  |      | 40.6 | 42. |
| 1900°               | 2            | 37.8             |      | 39.2 | 39.5 | 40.2  |      | 41.5 | 41.6 | 41.5  |      | 39.8 | 41. |
|                     | 4            | 37.5             |      | 38.8 | 38.3 | 40.1  |      | 41.4 | 41.0 | 39.6  |      | 40.9 | 41. |
|                     | 8            | 37.5             |      | 37.4 | 38.3 | 38.6  |      | 40.0 | 41.5 | 39.8  |      | 40.6 | 40. |
| 2000°               | 2            | 36.2             |      | 37.2 | 37.2 | 38.2  |      | 39.3 | 39.6 | 40.5  |      | 41.8 | 41. |
|                     | 4            | 35.8             |      | 36.9 | 36.6 | 36.2  |      | 39.1 | 38.9 | 37.0  |      | 40.1 | 40. |
|                     | 8            | 34.1             |      | 34.6 | 34.9 | 35.4  |      | 38.6 | 38.8 | 35.7  |      | 37.7 | 40. |
| 2100°               | 2            | 33.1             |      | 33.8 | 34.1 | 34.3  |      | 36.8 | 39.1 | 36.0  |      | 38.1 | 40. |
|                     | 4            | 31.9             |      | 33.3 | 31.1 | 33.3  |      | 35.3 | 37.8 | 37.2  |      | 39.7 | 40. |
|                     | 8            | 30.8             |      | 32.2 | 33.1 | 33.3  |      | 34.6 | 39.5 | 37.2  |      | 38.8 | 39. |
| 2200°               | 2            | 32.0             | 29.1 | 32.1 | 29.2 | 32.6  | 31.9 | 36.8 | 43.7 | 39.5  | 42.0 | 39.7 | 41. |
|                     | 4            | 30.9             | 28.8 | 28.3 | 28.5 | 29.2  | 30.5 | 36.8 | 43.3 | 40.7  | 41.0 | 42.4 | 41. |
|                     | 8            | 28.6             | 29.8 | 31.1 | 28.0 | 30.6  | 30.7 | 34.8 | 40.9 | 39.5  | 38.3 | 42.0 | 40. |
| 2250°               | 2            | 26.8             |      | 28.5 | 26.3 | 26.2  |      | 40.3 | 47.1 | 42.0  |      | 42.7 | 43. |
|                     | 4            | 27.8             |      | 27.4 | 30.5 | 28.7  |      | 38.6 | 44.3 | 41.8  |      | 43.2 | 42. |
|                     | 8            | 26.3             |      | 26.1 | 27.7 | 26.9  |      | 37.7 | 42.2 | 40.8  |      | 43.6 | 42. |

A



TABLE III

Hardness of Aged AR-213 Alloy ( $R_C$ )

| Aging Treatments |      |      |      |       |      |      |      |       |      |      |      |       |      |  |  |
|------------------|------|------|------|-------|------|------|------|-------|------|------|------|-------|------|--|--|
| 1400°            |      |      |      | 1600° |      |      |      | 1700° |      |      |      | 1800° |      |  |  |
| 4                | 8    | 16   | 32   | 4     | 8    | 16   | 32   | 4     | 8    | 16   | 32   | 4     | 8    |  |  |
| 40.7             |      | 42.0 | 42.8 | 41.1  |      | 42.6 | 41.9 | 41.8  |      | 41.4 | 40.0 |       |      |  |  |
| 39.3             |      | 42.2 | 41.2 | 41.0  |      | 41.6 | 41.4 | 41.3  |      | 41.4 | 39.7 |       |      |  |  |
| 39.5             |      | 41.7 | 42.0 | 41.0  |      | 40.6 | 42.3 | 40.7  |      | 39.2 | 40.9 |       |      |  |  |
| 40.2             |      | 41.5 | 41.6 | 41.5  |      | 39.8 | 41.9 | 39.7  |      | 40.8 | 36.3 | 38.9  |      |  |  |
| 40.1             |      | 41.4 | 41.0 | 39.6  |      | 40.9 | 41.0 | 40.4  |      | 39.9 | 39.1 | 39.0  |      |  |  |
| 38.6             |      | 40.9 | 41.5 | 39.8  |      | 41.0 | 40.8 | 40.2  |      | 38.9 | 38.9 | 39.5  |      |  |  |
| 38.2             |      | 39.2 | 38.6 | 40.5  |      | 40.8 | 40.3 | 40.1  |      | 39.1 | 40.1 | 37.6  |      |  |  |
| 36.2             |      | 39.1 | 38.9 | 37.0  |      | 40.1 | 40.0 | 39.0  |      | 39.9 | 39.5 | 37.4  |      |  |  |
| 35.4             |      | 38.6 | 38.8 | 35.7  |      | 37.7 | 40.0 | 35.6  |      | 39.2 | 38.3 | 36.8  |      |  |  |
| 34.3             |      | 36.8 | 39.1 | 36.0  |      | 38.1 | 40.5 | 38.2  |      | 39.7 | 39.5 | 37.8  |      |  |  |
| 33.3             |      | 35.3 | 37.8 | 37.2  |      | 39.7 | 40.0 | 39.4  |      | 37.9 | 37.8 | 37.1  |      |  |  |
| 33.3             |      | 34.6 | 39.5 | 37.2  |      | 38.8 | 39.3 | 36.9  |      | 38.9 | 37.3 | 37.8  |      |  |  |
| 32.6             | 31.9 | 36.8 | 43.7 | 39.5  | 42.0 | 39.7 | 41.7 | 39.2  | 38.9 | 38.4 | 39.1 | 36.4  | 38.0 |  |  |
| 29.2             | 30.5 | 36.8 | 43.3 | 40.7  | 41.0 | 42.4 | 41.5 | 38.3  | 38.8 | 37.9 | 38.8 | 34.9  | 37.4 |  |  |
| 30.6             | 30.7 | 34.8 | 40.9 | 39.5  | 38.3 | 42.0 | 40.2 | 37.9  | 38.6 | 36.3 | 38.0 | 36.4  | 36.9 |  |  |
| 26.2             |      | 40.3 | 47.1 | 42.0  |      | 42.7 | 43.0 | 40.6  |      | 40.9 | 40.1 | 38.0  |      |  |  |
| 28.7             |      | 38.6 | 44.3 | 41.8  |      | 43.2 | 42.9 | 40.9  |      | 38.8 | 40.2 | 37.2  |      |  |  |
| 26.9             |      | 37.7 | 42.2 | 40.8  |      | 43.6 | 42.6 | 39.8  |      | 39.5 | 39.7 | 37.4  |      |  |  |

B

| 1700°                |                      |                      |                      | 1800°                |                      |                      |                      | 1900°                |                      |                      |                      |
|----------------------|----------------------|----------------------|----------------------|----------------------|----------------------|----------------------|----------------------|----------------------|----------------------|----------------------|----------------------|
| 4                    | 8                    | 16                   | 32                   | 4                    | 8                    | 16                   | 32                   | 4                    | 8                    | 16                   | 32                   |
| 41.8<br>41.3<br>40.7 |                      | 41.4<br>41.4<br>39.2 | 40.0<br>39.7<br>40.9 |                      |                      |                      |                      |                      |                      |                      |                      |
| 39.7<br>40.4<br>40.2 |                      | 40.8<br>39.9<br>38.9 | 36.3<br>39.1<br>38.9 | 38.9<br>39.0<br>39.5 |                      | 39.4<br>39.2<br>36.5 | 37.5<br>39.1<br>39.5 |                      |                      |                      |                      |
| 40.1<br>39.0<br>35.6 |                      | 39.1<br>39.9<br>39.2 | 40.1<br>39.5<br>38.3 | 37.6<br>37.4<br>36.8 |                      | 37.7<br>38.1<br>37.5 | 37.8<br>38.0<br>36.9 | 33.7<br>35.5<br>36.1 |                      | 36.0<br>36.8<br>34.8 | 35.8<br>35.3<br>35.1 |
| 38.2<br>39.4<br>36.9 |                      | 39.7<br>37.9<br>38.9 | 39.5<br>37.8<br>37.3 | 37.8<br>37.1<br>37.8 |                      | 38.0<br>37.0<br>36.7 | 38.0<br>37.4<br>36.3 | 36.5<br>35.6<br>34.3 |                      | 34.0<br>35.3<br>33.3 | 34.3<br>34.0<br>33.3 |
| 39.2<br>38.3<br>37.9 | 38.9<br>38.8<br>38.6 | 38.4<br>37.9<br>36.3 | 39.1<br>38.8<br>38.0 | 36.4<br>34.9<br>36.4 | 38.0<br>37.4<br>36.9 | 37.5<br>36.2<br>35.9 | 37.5<br>36.5<br>36.0 | 34.7<br>33.7<br>36.7 | 35.2<br>34.9<br>34.3 | 33.4<br>33.5<br>33.3 | 34.0<br>33.3<br>31.9 |
| 40.6<br>40.9<br>39.8 |                      | 40.9<br>38.8<br>39.5 | 40.1<br>40.2<br>39.7 | 38.0<br>37.2<br>37.4 |                      | 37.1<br>37.4<br>36.4 | 37.5<br>37.2<br>36.0 | 35.5<br>34.3<br>34.9 |                      | 33.8<br>34.1<br>34.5 | 35.0<br>34.4<br>32.8 |

C

TABLE IV  
X-Ray Diffraction Data for Extracted Particles<sup>a</sup>

| <u>Observed</u> | <u>Lattice plane<br/>Spacing (Å)</u> | <u>Calculated<sup>c</sup></u> | <u>Relative<br/>Intensity<sup>b</sup></u> | <u>Probable<br/>Structure</u> | <u>Miller<br/>Indices</u> |
|-----------------|--------------------------------------|-------------------------------|---|-------------------------------|---------------------------|
|                 |                                      | <u>I</u>                      |   |                               | <u>(hkl)</u>              |
| 2.90            | 2.85                                 | 17                            |   | CoAl                          | (100)                     |
| 2.64            | 2.64                                 | 100                           |   | ZrN                           | (111)                     |
| 2.28            | 2.28                                 | 88                            |   | ZrN                           | (200)                     |
| 2.23            |                                      | 14                            |   | Unknown                       | ----                      |
| 2.04            | 2.02                                 | 88                            |   | CoAl                          | (110)                     |
| 1.61            | 1.61                                 | 57                            |   | ZrN                           | (220)                     |
| 1.44            | 1.43                                 | 21                            |   | CoAl                          | (200)                     |
| 1.37            | 1.38                                 | 62                            |   | ZrN                           | (311)                     |
| 1.31            | 1.32                                 | 29                            |   | ZrN                           | (222)                     |
| 1.17            | 1.17                                 | 59                            |   | CoAl                          | (211)                     |

a. Extractions obtained from AR-213 solution treated at 2200° for 8 hours.

b. Based on a value of 100 for the highest peak

c. Based upon ASTM card file for ZrN and upon AiResearch laboratory data for CoAl.

TABLE V

X-Ray Fluorescent Analysis of Extracted Particles<sup>a</sup>

| <u>Element</u> | <u>X-Ray Line Designation</u> | <u>Matrix</u> | <u>Intensity<sup>b</sup></u> | <u>Extractions</u> |
|----------------|-------------------------------|---------------|------------------------------|--------------------|
| Zr             | KAl                           | 3             |                              | 51                 |
| Ta             | LAl                           | 3             |                              | 72                 |
| W              | LAl                           | 6             |                              | 6                  |
| Co             | KA                            | 200           |                              | 90                 |
| Fe             | KA                            | 9             |                              | 1                  |
| Cr             | KA                            | 26            |                              | 6                  |

a. Extractions obtained from AR-213 solution treated at 2200° F for 8 hours.

b. Intensity units simply represent the peak heights as recorded on the chart paper.

**APPENDIX B**

**HEAT TREATMENT CURVES**

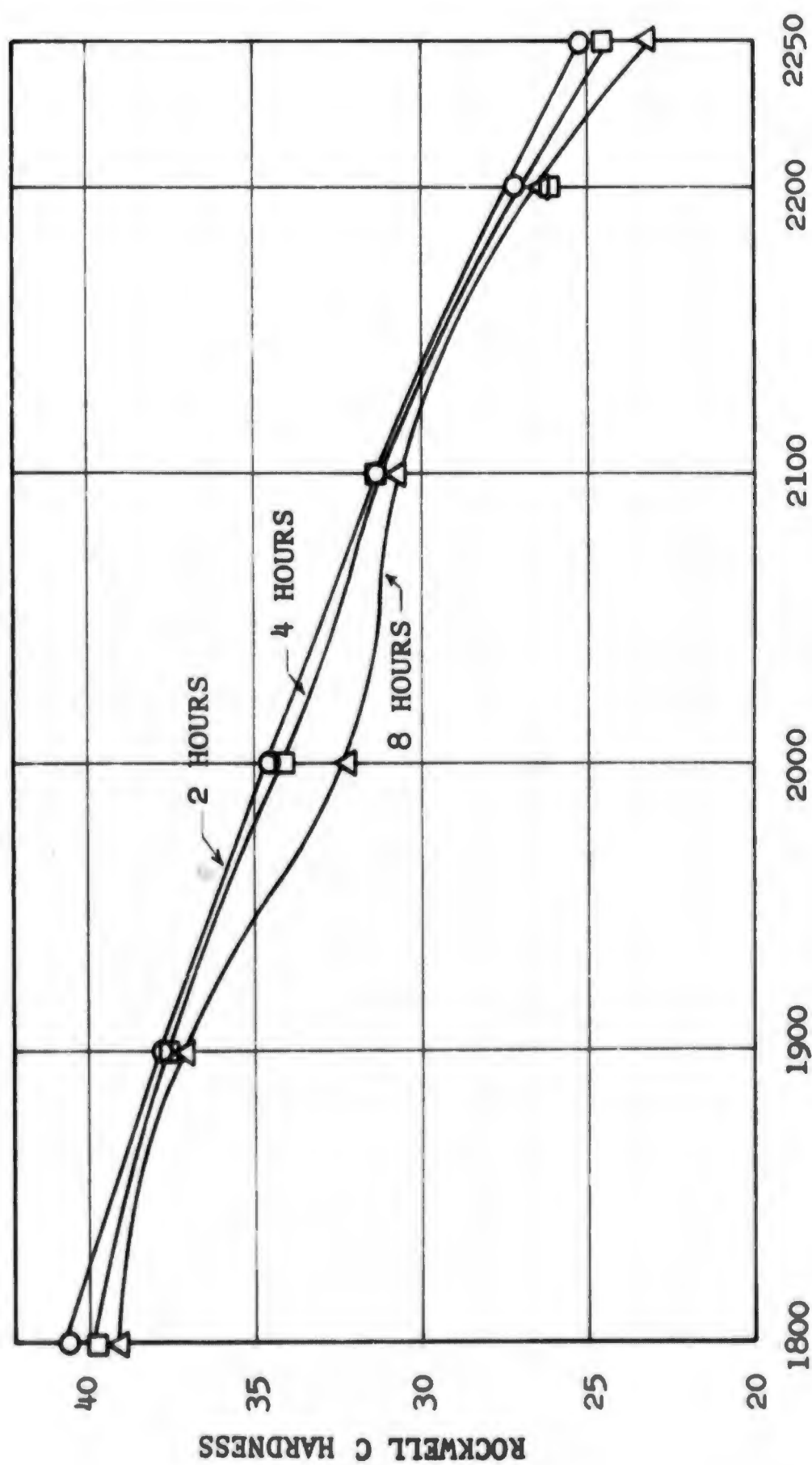


Figure 1. Hardness Versus Solution Heat Treat Temperature

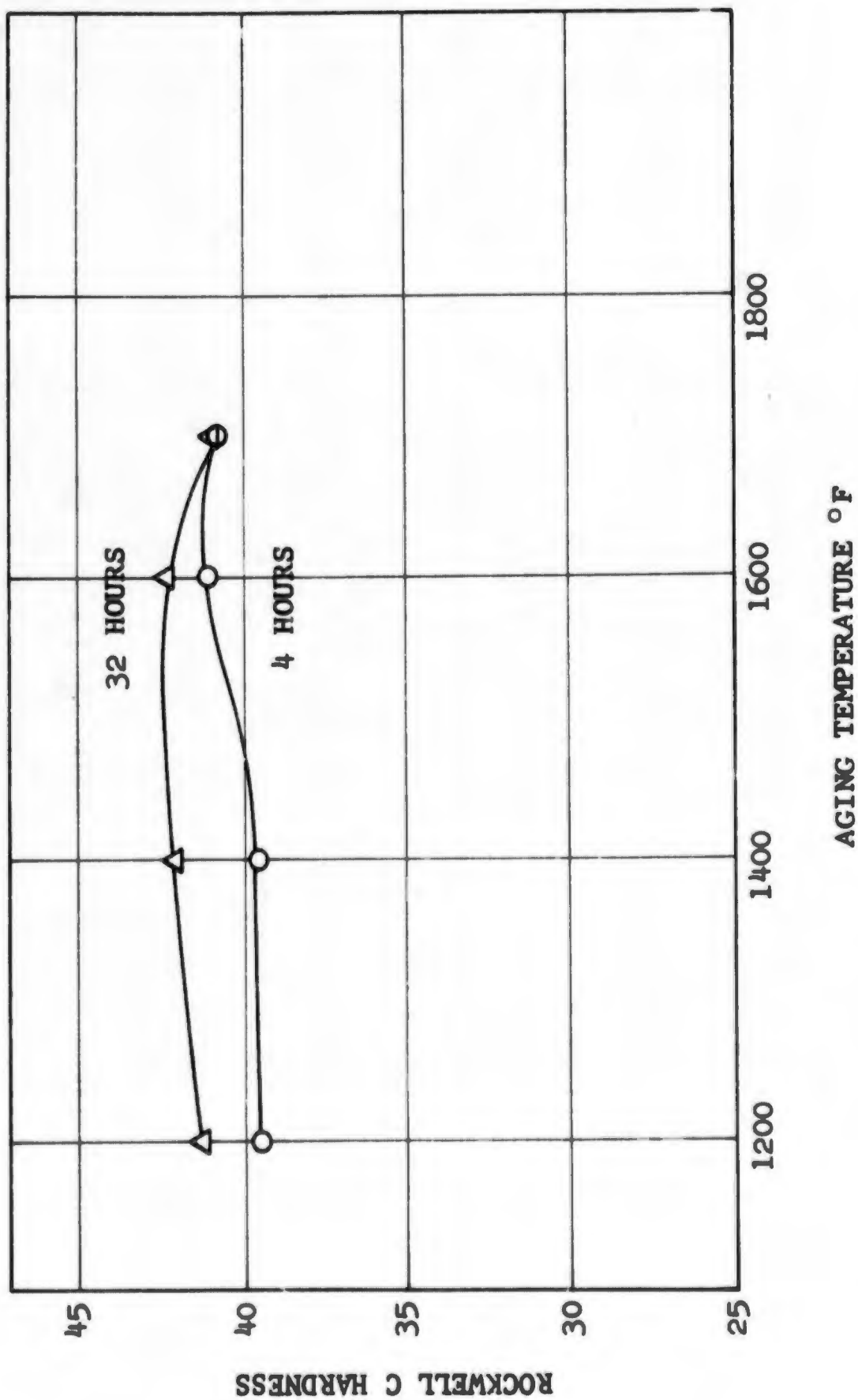


Figure 2. Hardness Versus Aging Temperature for AR-213 Solution Treated at 1800° F for 8 hours

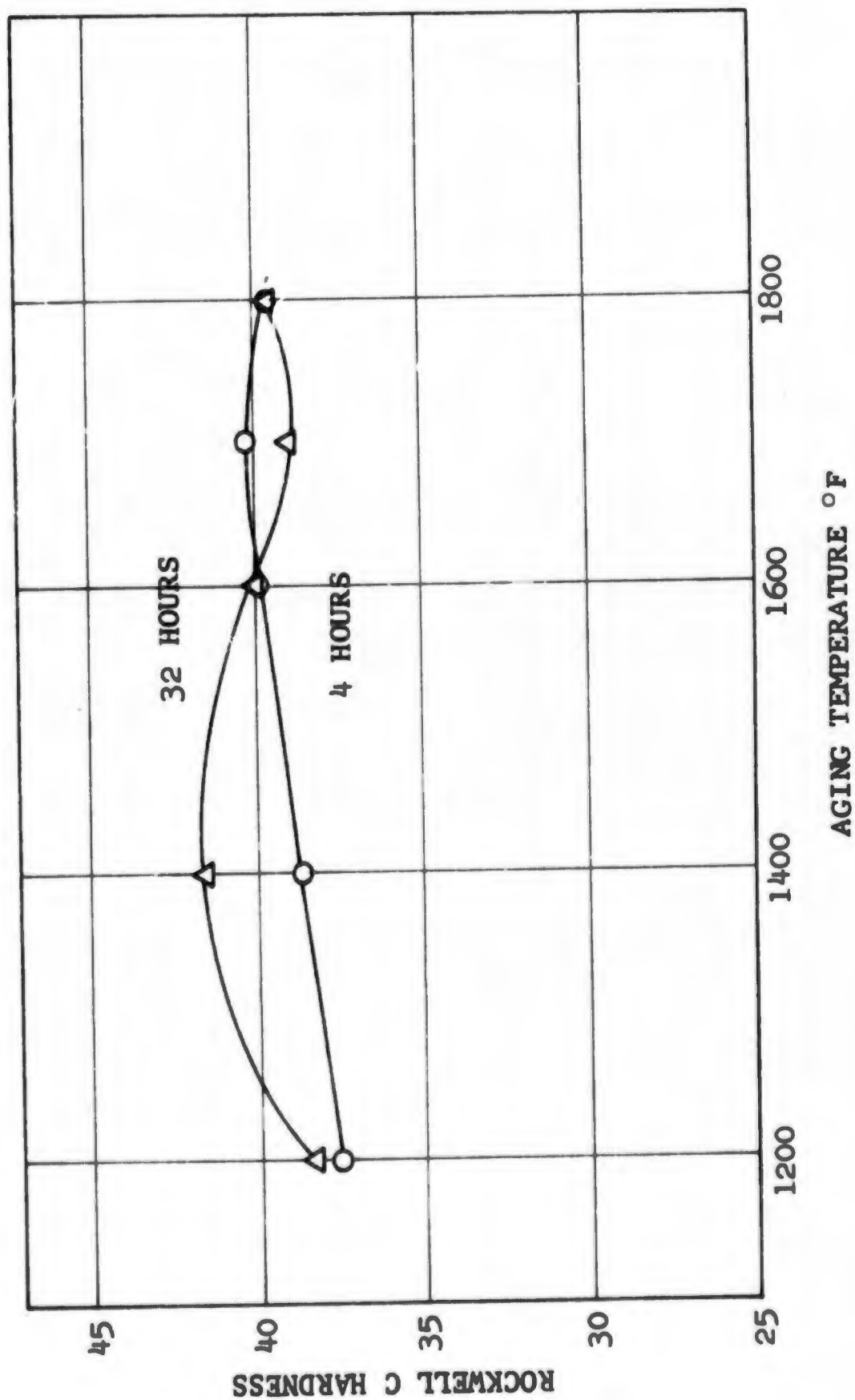


Figure 3. Hardness Versus Aging Temperature for AR-213 Solution Treated at 1900° F for 8 hours



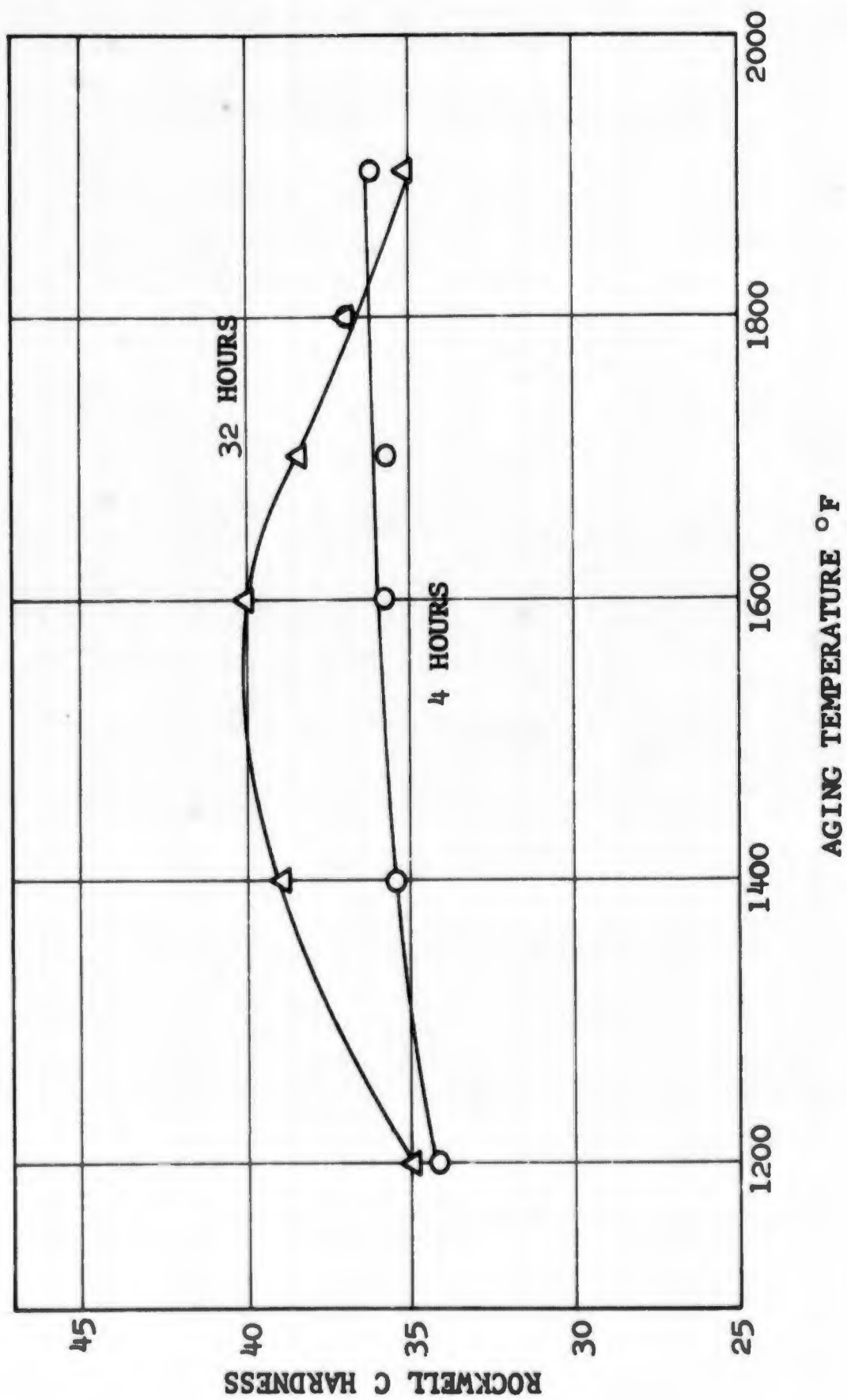


Figure 4. Hardness Versus Aging Temperature for AR-213 Solution Treated at 2000° F for 8 hours

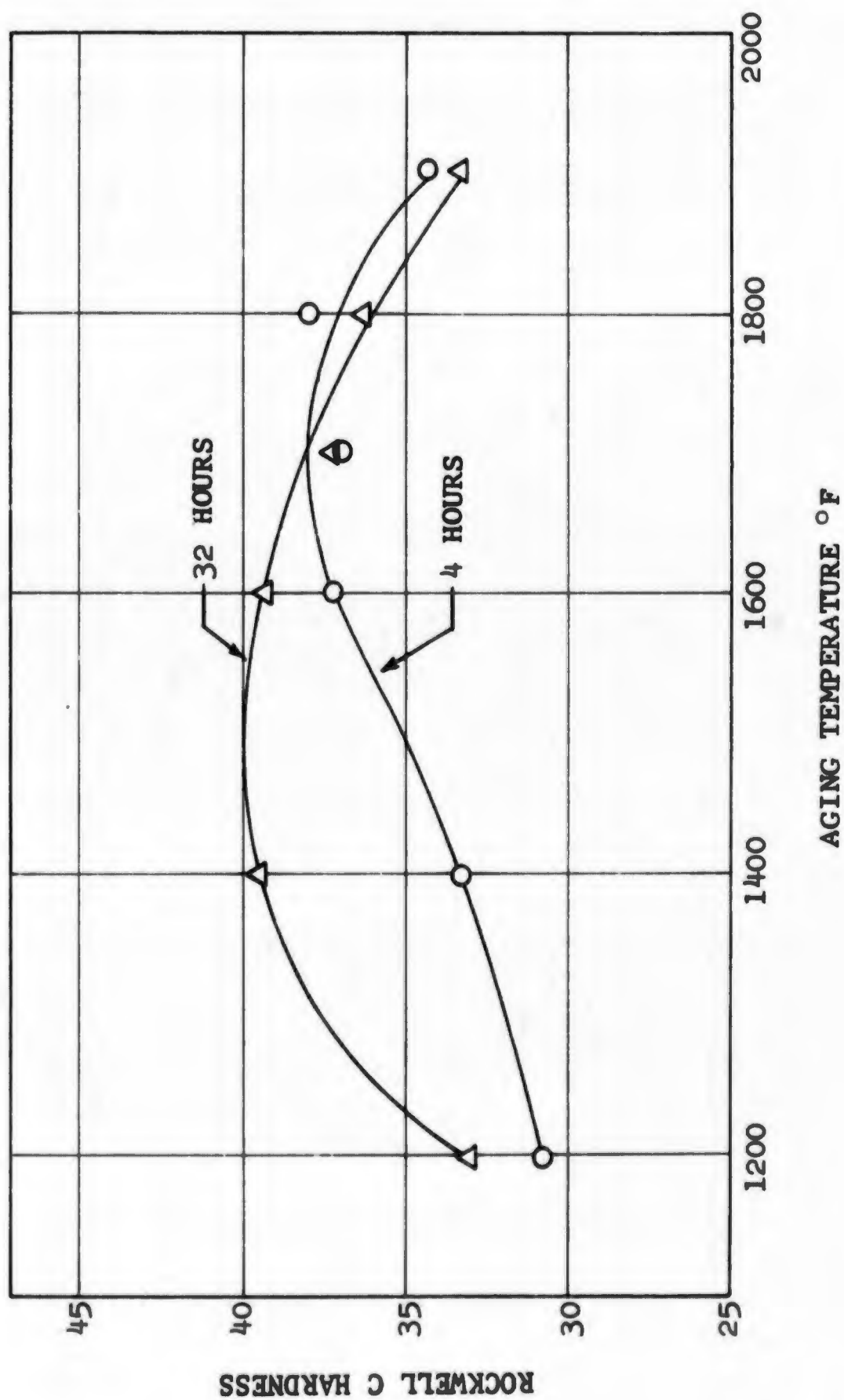


Figure 5. Hardness Versus Aging Temperature for AR-213 Solution Treated at 2100° F for 8 hours

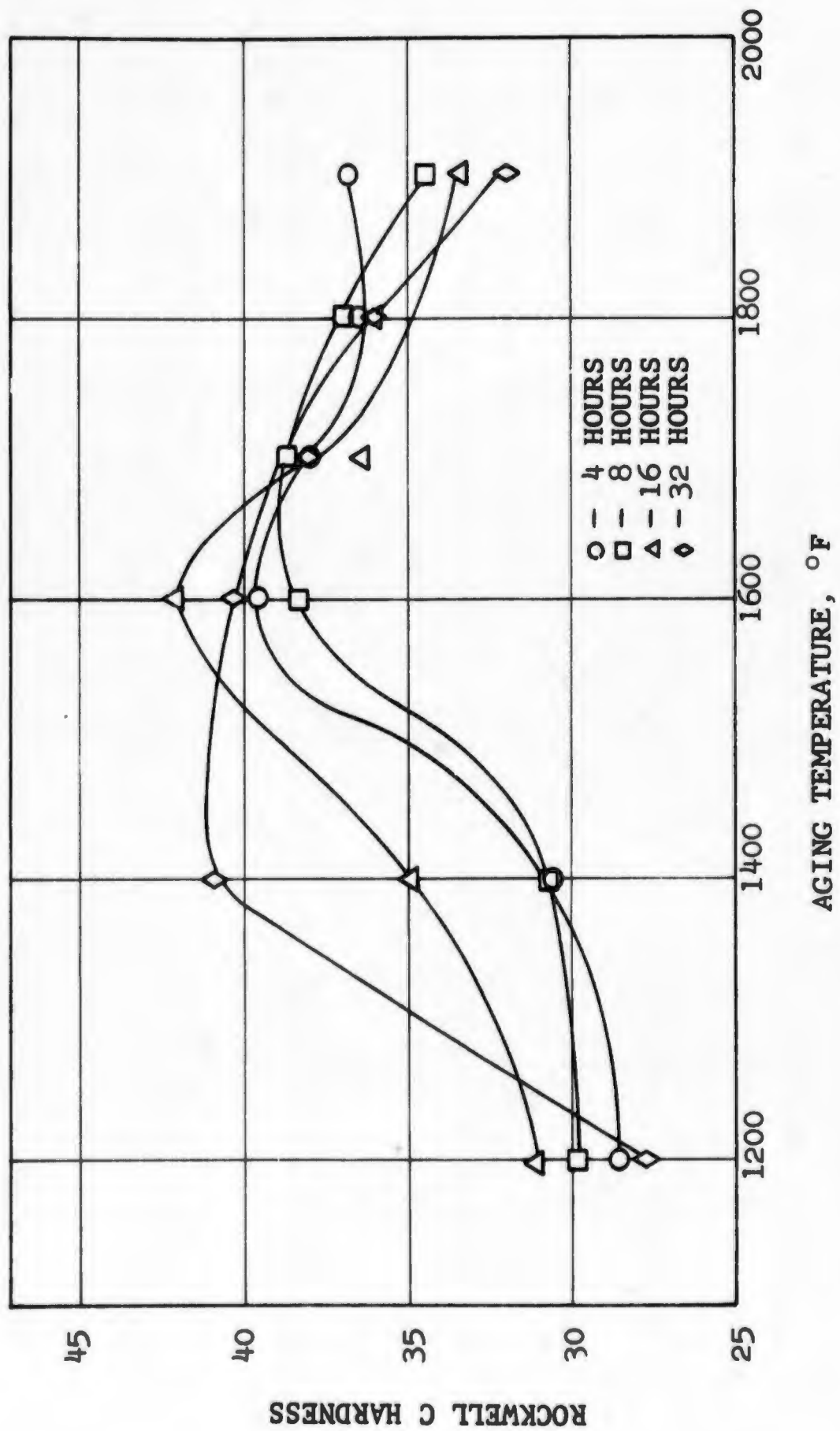


Figure 6. Hardness Versus Aging Temperature for AR-213 Solution Treated at 2200° F for 8 hours

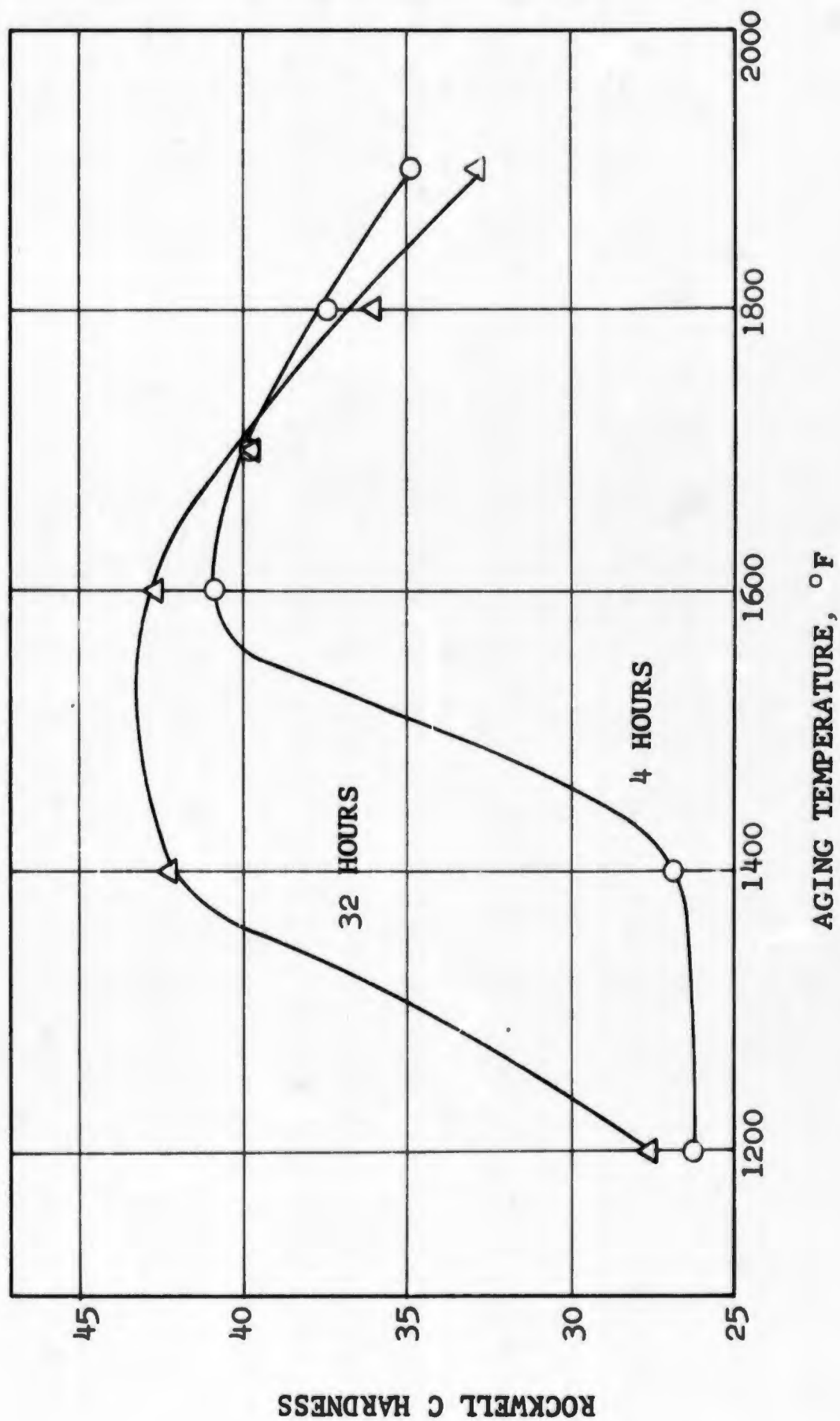


Figure 7. Hardness Versus Aging Temperature for AR-213 Solution Treated at 2250° F for 8 hours

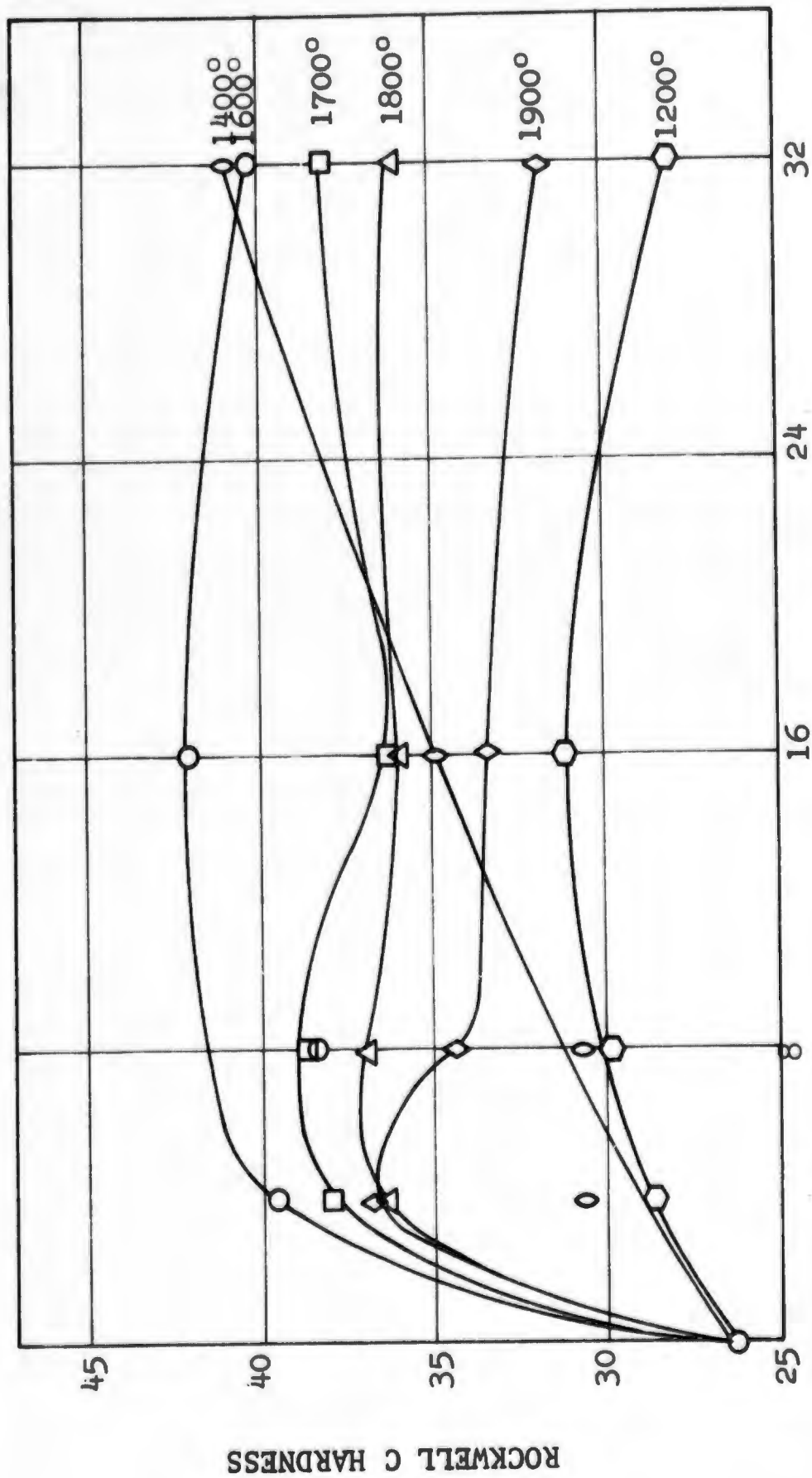


Figure 8. Hardness Versus Aging Time and Temperature for AR-213 Solution Treated at 2200° F for 8 hours

## APPENDIX C

### OPTICAL AND ELECTRON MICROSCOPY PROCEDURES

## 1. Optical Metallography

- a. The specimens were mounted in lucite or bakelite and ground on 80 through 600 grit papers.
- b. Initial polishing was done on a felt wheel using Linde "A" alumina.
- c. Final polishing was accomplished on a vibratory polisher employing a slurry of Linde "B" alumina. A polishing time of 2 to 4 hours was employed, with longer times accentuating the relief between the hard phase and the softer matrix.
- d. The specimens were etched for 10 to 20 seconds in a solution composed of 40 percent  $H_2O$ , 30 percent conc.  $HCl$ , and 30 percent of a 3%  $H_2O_2$  solution. The  $HCl$  was added to the  $H_2O_2$  and allowed to stand for 15 minutes prior to adding the water.

## 2. Electron Microscopy

- a. Steps a through d above were repeated except that the etching time was reduced to 7 to 10 seconds.

- b. The specimen surface was then cleaned twice by brushing a solution of cellulose acetate over the surface and then pressing a cellulose acetate tape on the surface. The tape was stripped off when dry and discarded.
- c. The replica was initiated by placing several drops of a solution of polystyrene dissolved in ethylene dichloride on the cleaned surface. The polystyrene film was allowed to dry at least 15 hours prior to being stripped off. Two precautions necessitated this long drying period. First, this solution dissolved a lucite mount but not a bakelite one, and second, if a too viscous polystyrene solution was used "pulls" occurred when the polystyrene was stripped which led to artifacts in the final replica.
- d. The polystyrene film was then inverted, placed in a Mikros vacuum evaporator, and shadowed first with platinum-palladium at a  $45^{\circ}$  angle and then carbon at a  $90^{\circ}$  angle. Prior to the evaporation it was



imperative to allow the polystyrene film to recover from the stretching it received during the stripping from the surface. Unless allowance for this stretching was made, the shadowed replica crazed during the next cutting operation. A 12-hour interval between stripping and shadowing was sufficient to prevent the crazing.

- e. The shadowed replica was then cut into squares and placed, carbon side up, on the 400 mesh copper grids used to hold the replica in the Hitachi microscope.
- f. The grids were then placed on a screen which just touched the surface of an ethylene dichloride bath. This solution dissolved the polystyrene away from the underside of the carbon and left the shadowed carbon replica lying on the grid ready for viewing in the microscope.

## APPENDIX D

### OPTICAL AND ELECTRON MICROSCOPY PHOTOGRAPHS

The optical and electron microscopy photographs represent a series consisting of as-cast, as-cast plus solution treated, and as-cast plus solution treated plus aged specimens. All aged specimens received the "optimum" solution treatment of  $2200^{\circ}$  F for 8 hours. All agings were for 32 hours at the temperatures indicated.

Each specimen was etched with a solution of 40 percent  $H_2O$ , 30 percent concentrated HCl and 30 percent of a 3%  $H_2O_2$  solution.

The optical microscopy (Figs. 9 through 27) was done at 100 and 700 X and the pictures are printed at the original magnification. The electron microscopy photographs (Figs. 28 through 48) were taken at either 5000 or 10,000 X and were magnified 1.8 times for reproduction.

Figure 9. AR-213 Aged at 1200° F (unetched)  
700 X

This unetched specimen shows the typical location of the carbonitride phase at the interface of the matrix and primary CoAl.

Figure 10. AR-213 Aged at 1800° F (unetched)  
700 X

Note the black dot in the center of the triangular carbonitride phase. This dot is characteristic of nitrides high in carbon content. This phase is actually a distinctive pink.



Figure 11. As-Cast AR-213  
100 X

Typical cored casting showing primary CoAl in matrix.

Figure 12. As-Cast AR-213  
700 X

Same structure as above showing primary CoAl in a quite clean matrix.

Hardness -  $R_C$  25.7

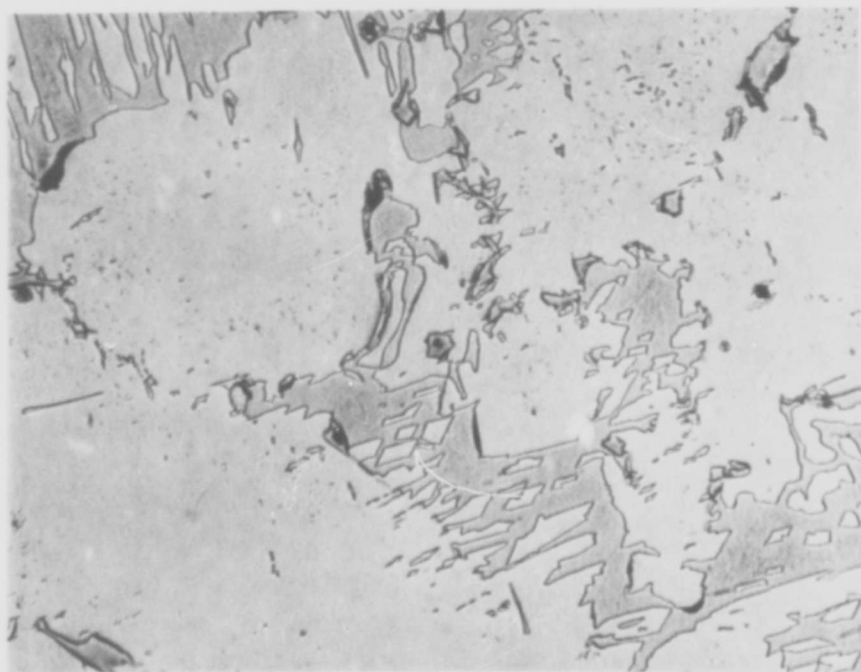
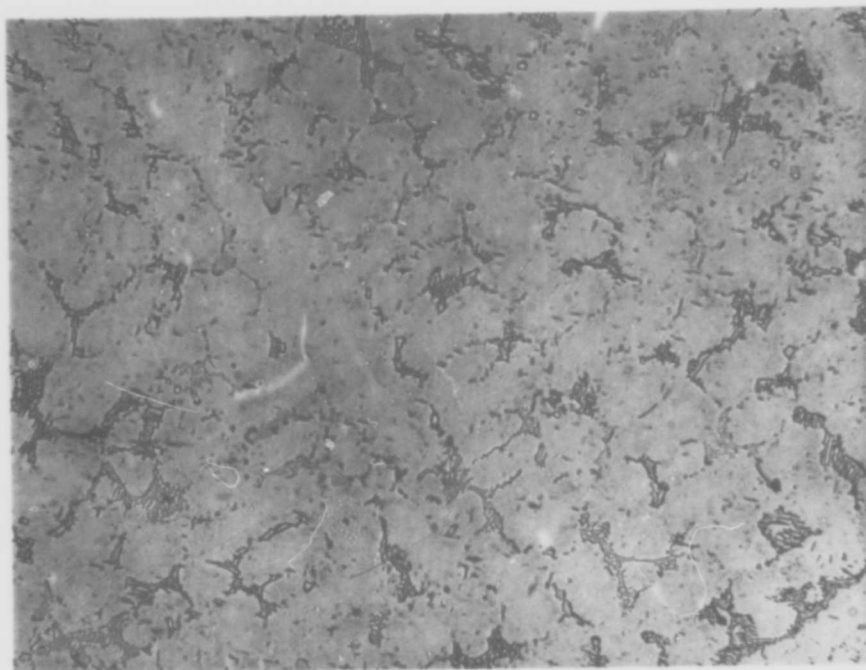


Figure 13. Solution Treated AR-213  
100 X

The carbonitride stringers are much more evident after solution treating. Otherwise, there is not much change from the as-cast condition.

Figure 14. Solution Treated AR-213  
700 X

Same structure as above showing primary CoAl.

Hardness -  $R_C$  26.3



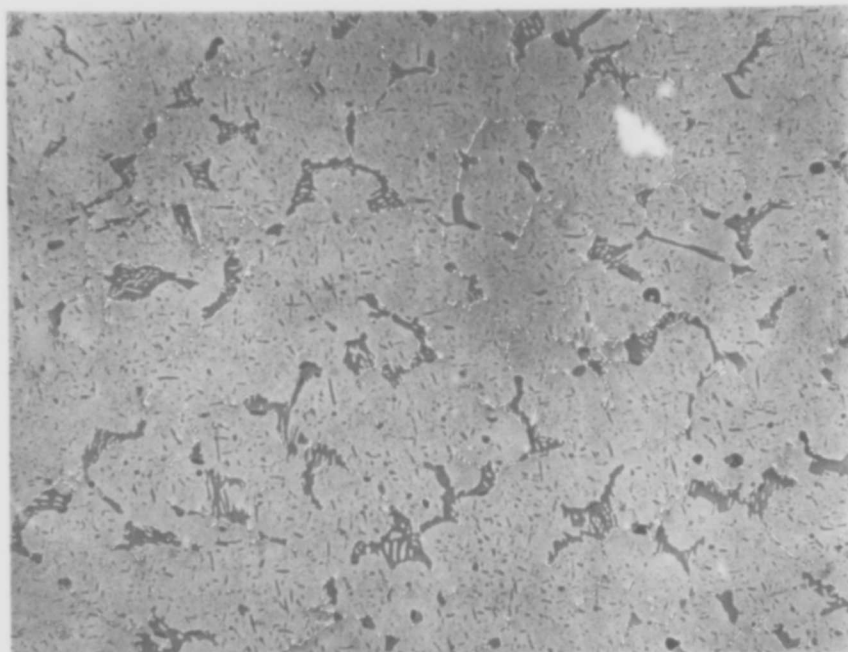


Figure 15. AR-213 Aged at 1200° F  
100 X

No change in microstructure from the solution treated condition.

Figure 16. AR-213 Aged at 1200° F  
700 X

The morphology of the primary CoAl has not yet changed. Note that at this aging temperature no precipitate has yet appeared. This corresponds to the absence of any significant hardness increase for this aging temperature.

Hardness -  $R_C$  28.0

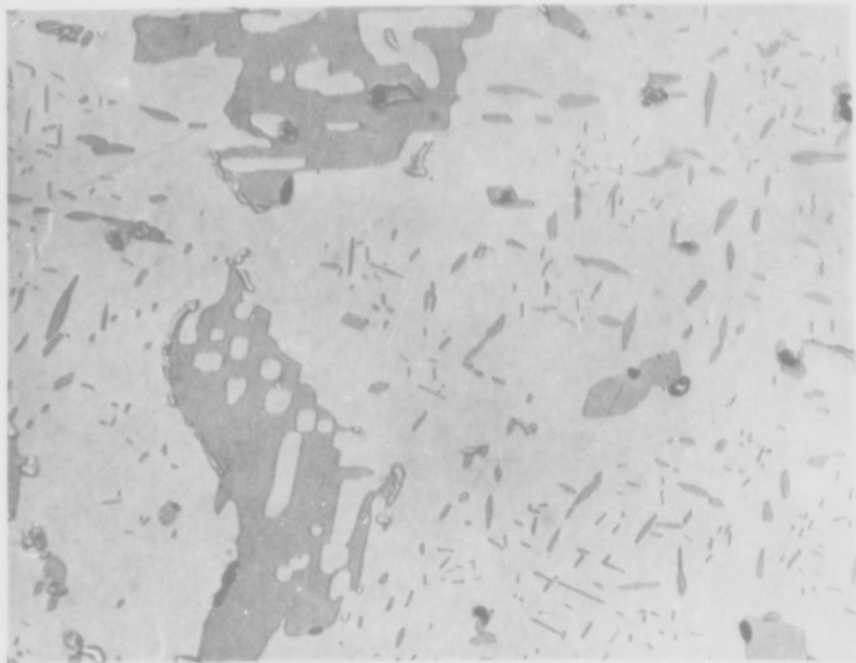
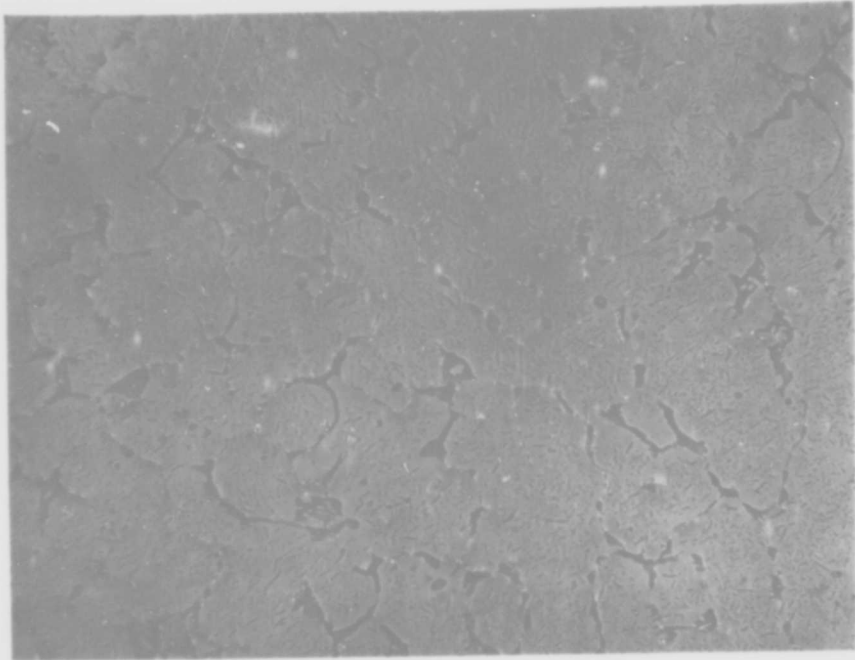


Figure 17. AR-213 Aged at 1400° F  
100 X

The appearance of the matrix at this magnification shows just a slight general darkening.

Figure 18. AR-213 Aged at 1400° F  
700 X

At this higher magnification a very fine general precipitate is evident. The precipitate is secondary CoAl. This microstructure corresponds to the maximum aged hardness.

Hardness -  $R_C$  40.9

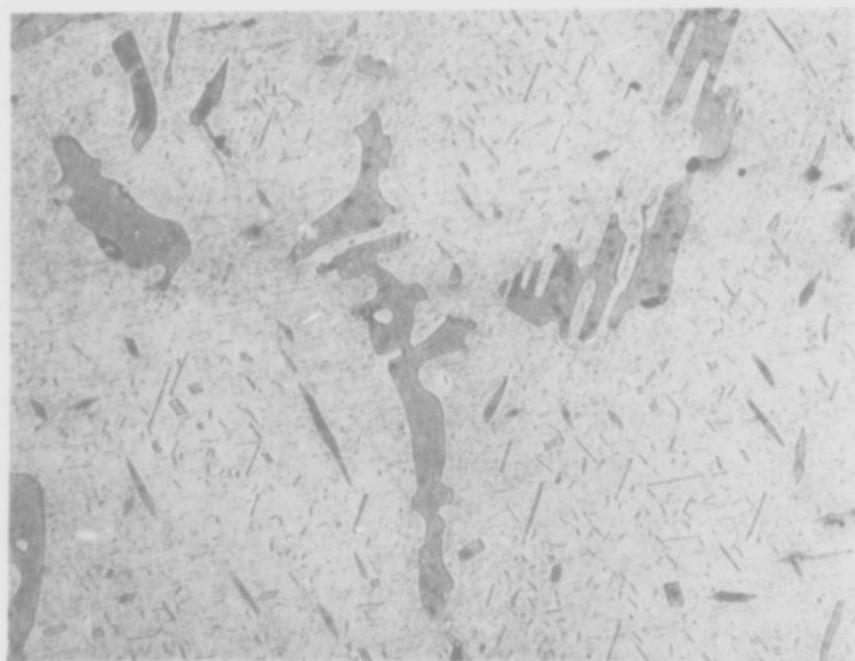


Figure 19. AR-213 Aged at 1600° F  
100 X

There is still not much change in microstructure at this magnification even at the higher aging temperature.

Figure 20. AR-213 Aged at 1600° F  
700 X

The general matrix precipitation is now quite well defined along preferred crystallographic directions.

Hardness -  $R_C$  40.2

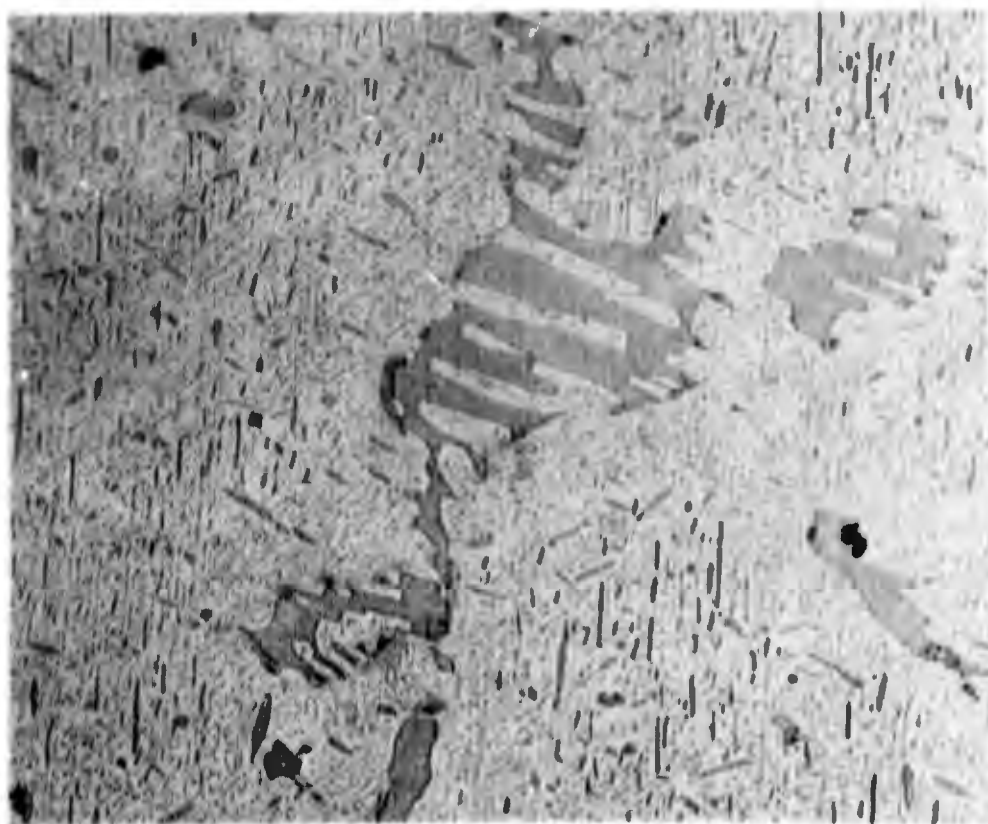
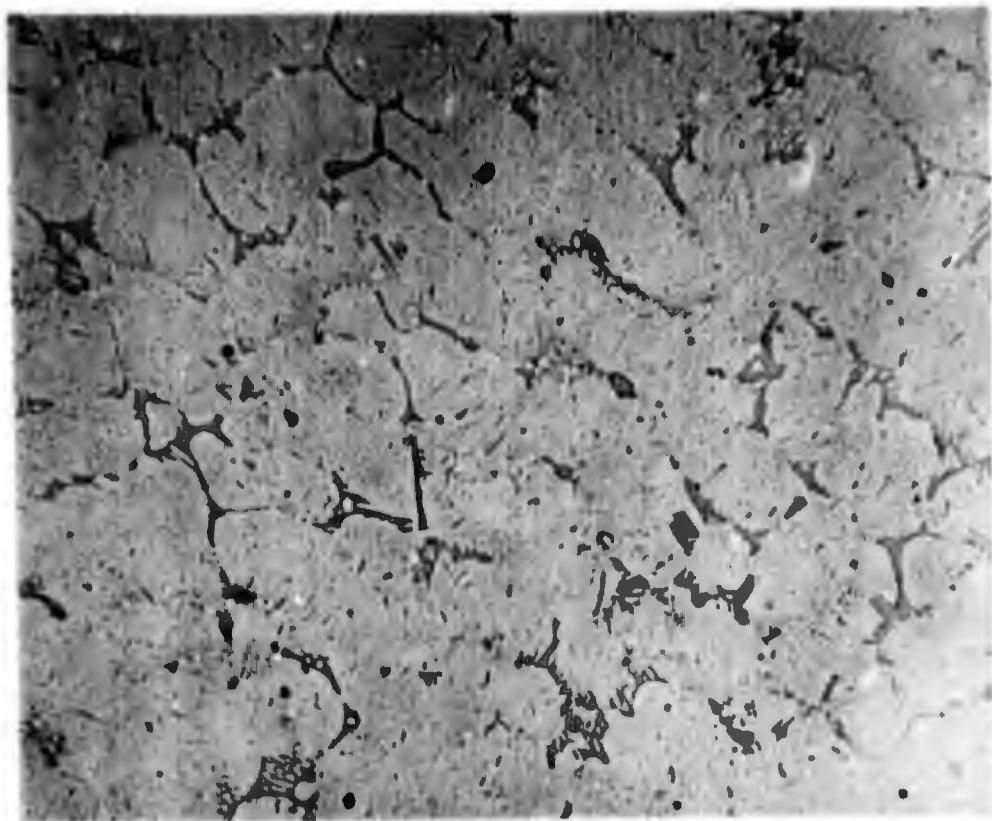


Figure 21. AR-213 Aged at 1700° F  
100 X

The precipitation in the matrix has coarsened enough to be visible at this magnification.

Figure 22. AR-213 Aged at 1700° F  
700 X

Not only has the matrix precipitate coarsened but the decomposition of the primary CoAl is now evident.

Hardness - R<sub>C</sub> 38.0



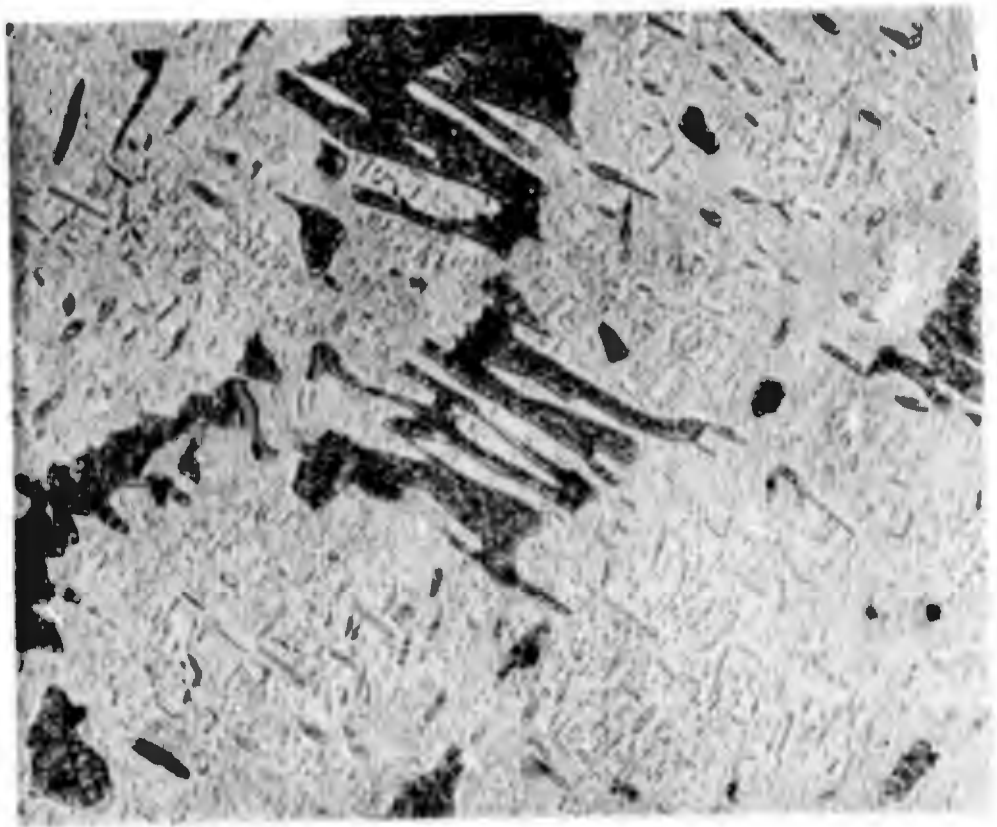
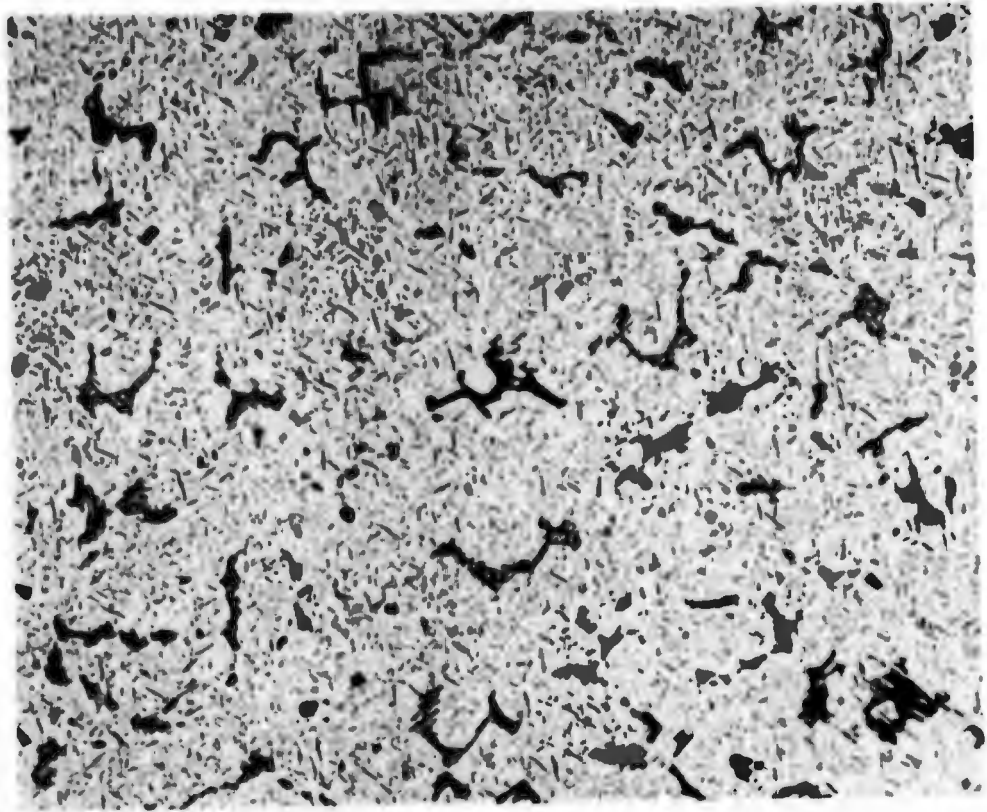


Figure 23. AR-213 Aged at 1800° F  
100 X

The matrix now exhibits a quite coarse general precipitate.

Figure 24. AR-213 Aged at 1800° F  
700 X

A high degree of coalescence of the precipitate is now evident.

Hardness -  $R_C$  36.0

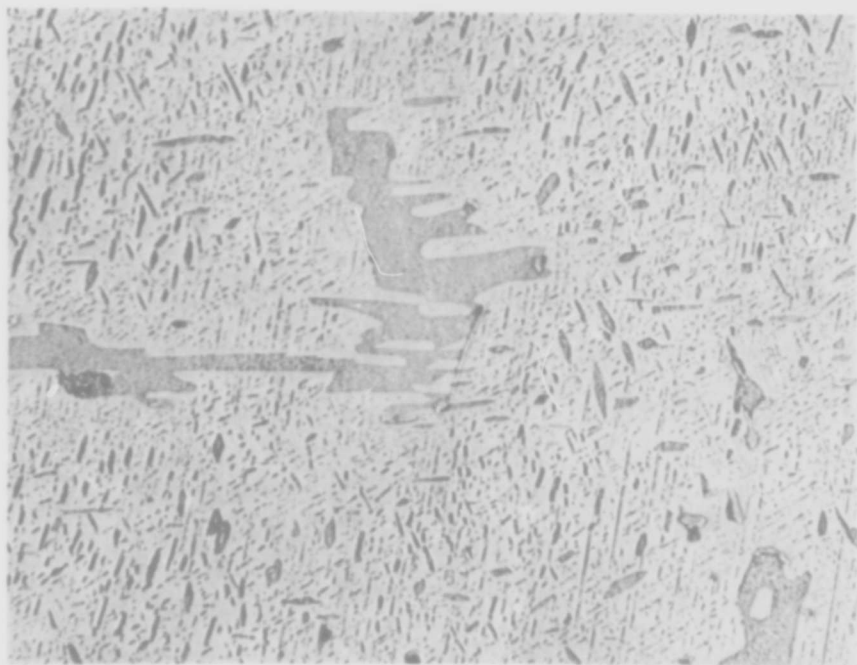
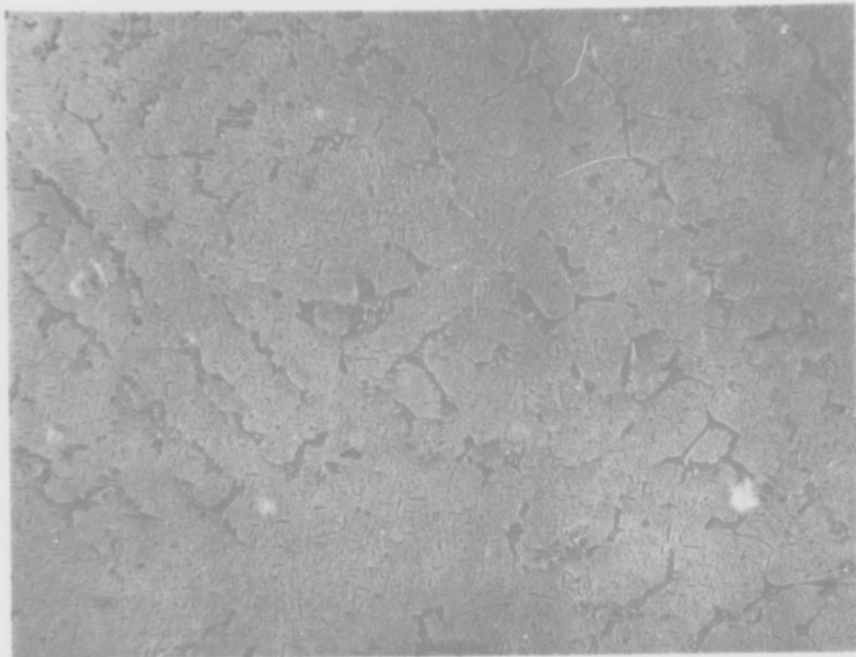


Figure 25. AR-213 Aged at 1900° F  
100 X

The overaging of the matrix precipitate and further decomposition of the primary CoAl are clearly shown.

Figure 26. AR-213 Aged at 1900° F  
700 X

Further coalescence of the precipitate is evident as is the decomposition of the primary CoAl. In addition, it appears that perhaps some of the precipitate has gone back into solution as evidenced by the large denuded zone around the primary CoAl phase.

Hardness -  $R_C$  31.9

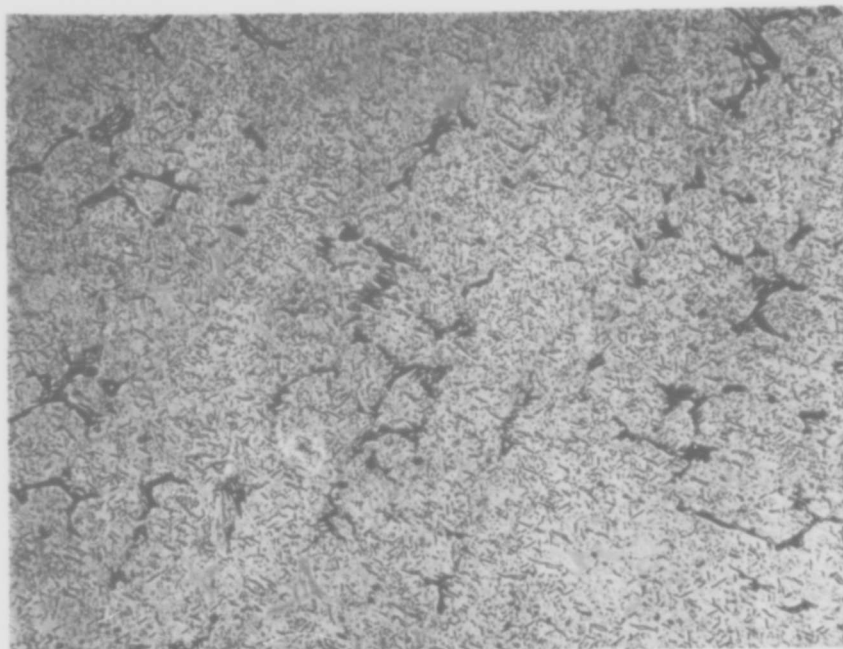


Figure 27. Solution Treated AR-213 - Carbide Stringers

The long stringer was determined by microprobe analysis to contain a high percentage of tantalum. Its composition was, therefore, assumed to be TaC. The black circular spot was that caused by the microprobe during examination.

Magnification: 100 X      Enlarged: 1.8 times for reproduction

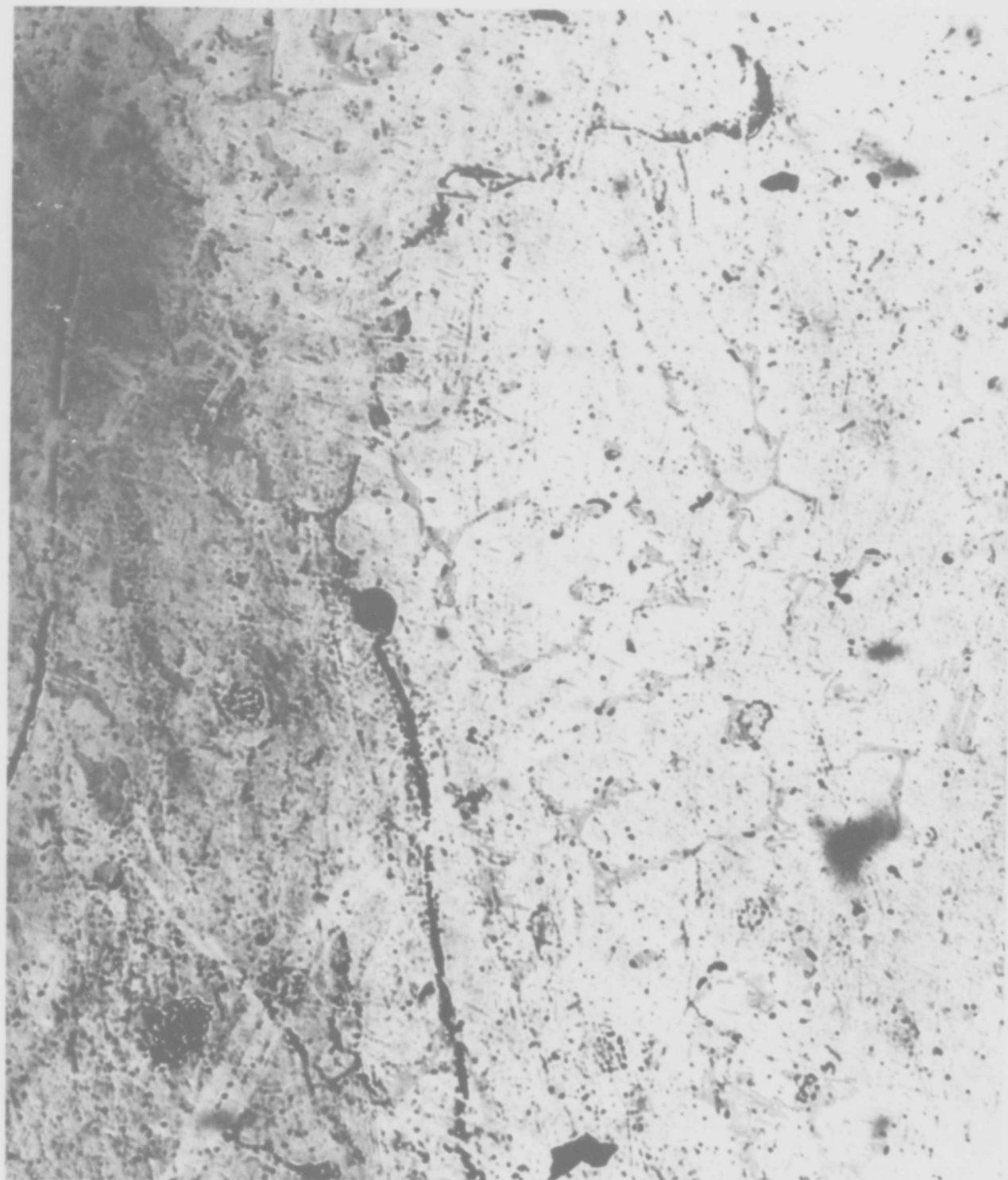


Figure 28. As-Cast AR-213 - General Matrix

Typical view of cast matrix. The larger particles are CoAl.

Magnification: 5000 X





Figure 29. As-Cast AR-213 - Primary CoAl in Matrix

The homogeneous areas are primary CoAl in the matrix.  
The rhombohedral shape is characteristic for this phase.

Magnification: 5000 X



Figure 30. As-Cast AR-213 - Matrix, CoAl and Carbonitride

This specimen shows primary CoAl sandwiched between a carbonitride particle on the left and the matrix. This position for the carbonitride is typical in this alloy. Its color is a distinctive pink.

Magnification: 10,000 X



Figure 31. Solution Treated AR-213 - General Matrix

Typical view of matrix with several CoAl particles.

Magnification: 5000 X

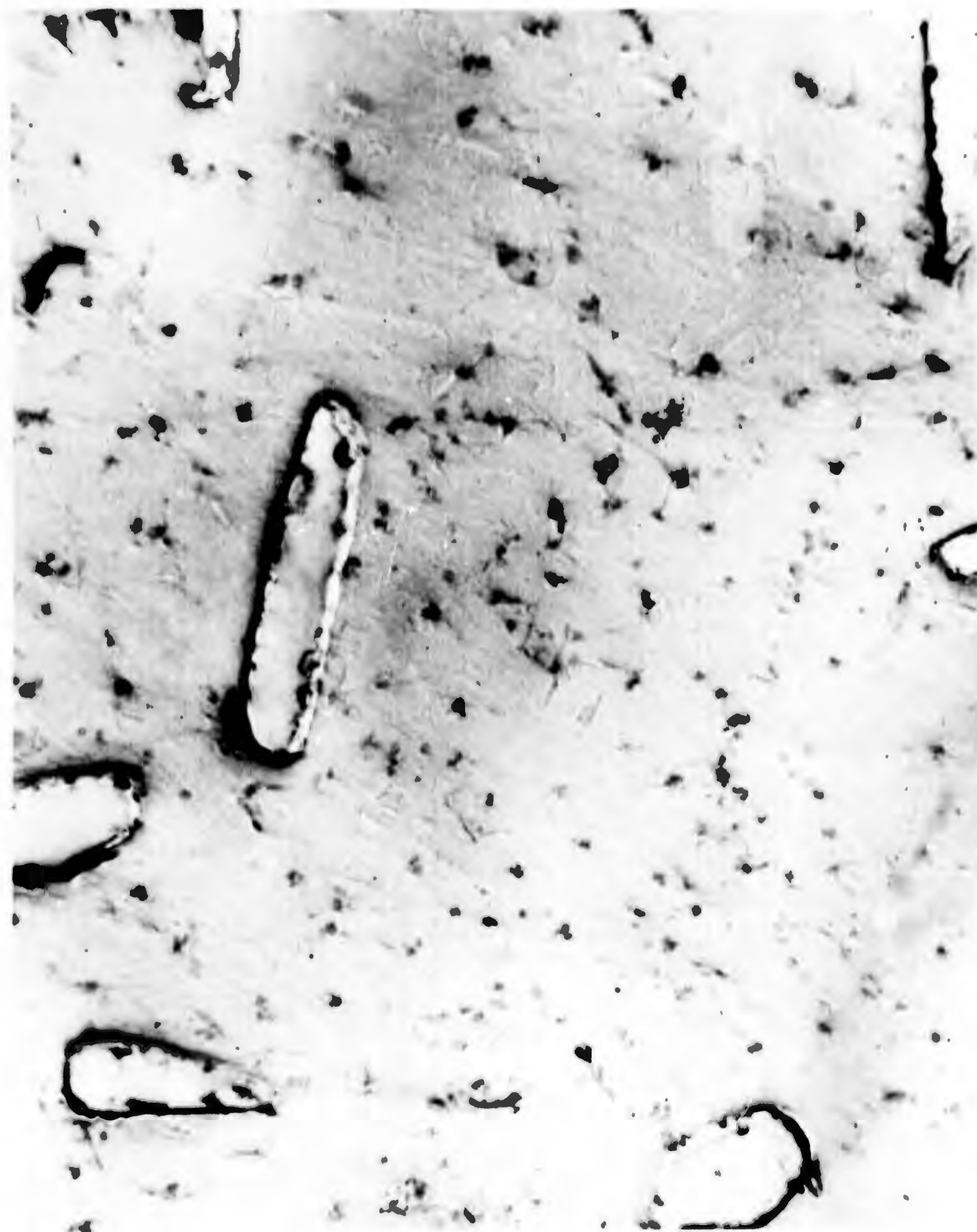


Figure 3^      Solution Treated AR-213 - General Matrix

Less typical view of matrix showing several CoAl  
particles in the "clean" matrix.

Magnification: 5000 X





Figure 33. Solution Treated AR-213 - General Matrix

Typical view of CoAl in the matrix. The long scratch running through the lower end of the CoAl phase shows its greater hardness with respect to the matrix. The star shaped indentations are unexplained.

Magnification: 5000 X

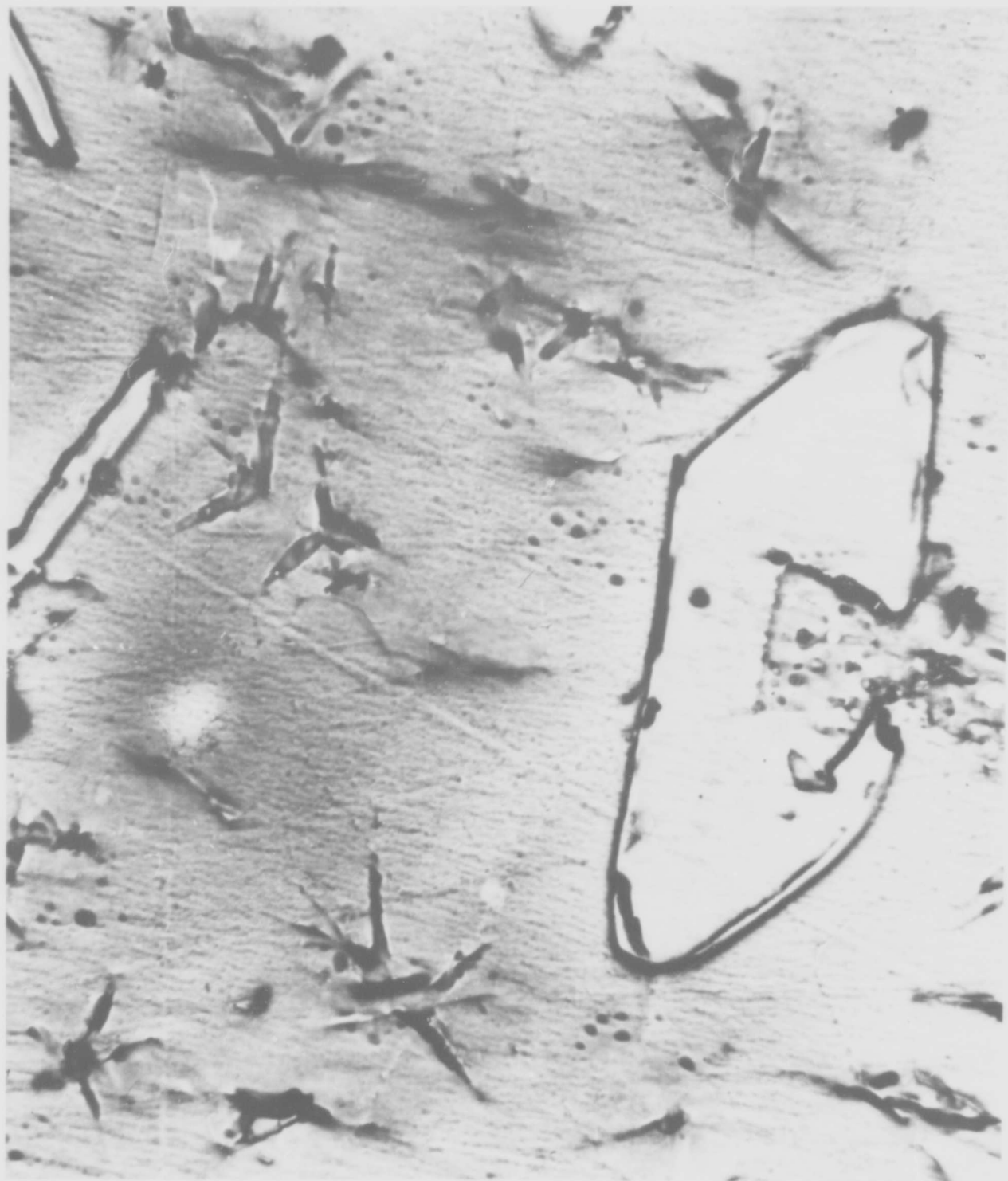


Figure 34. AR-213 Aged at 1200<sup>o</sup> F - General Matrix

Typical view of primary CoAl in the matrix.

Magnification: 5000 X

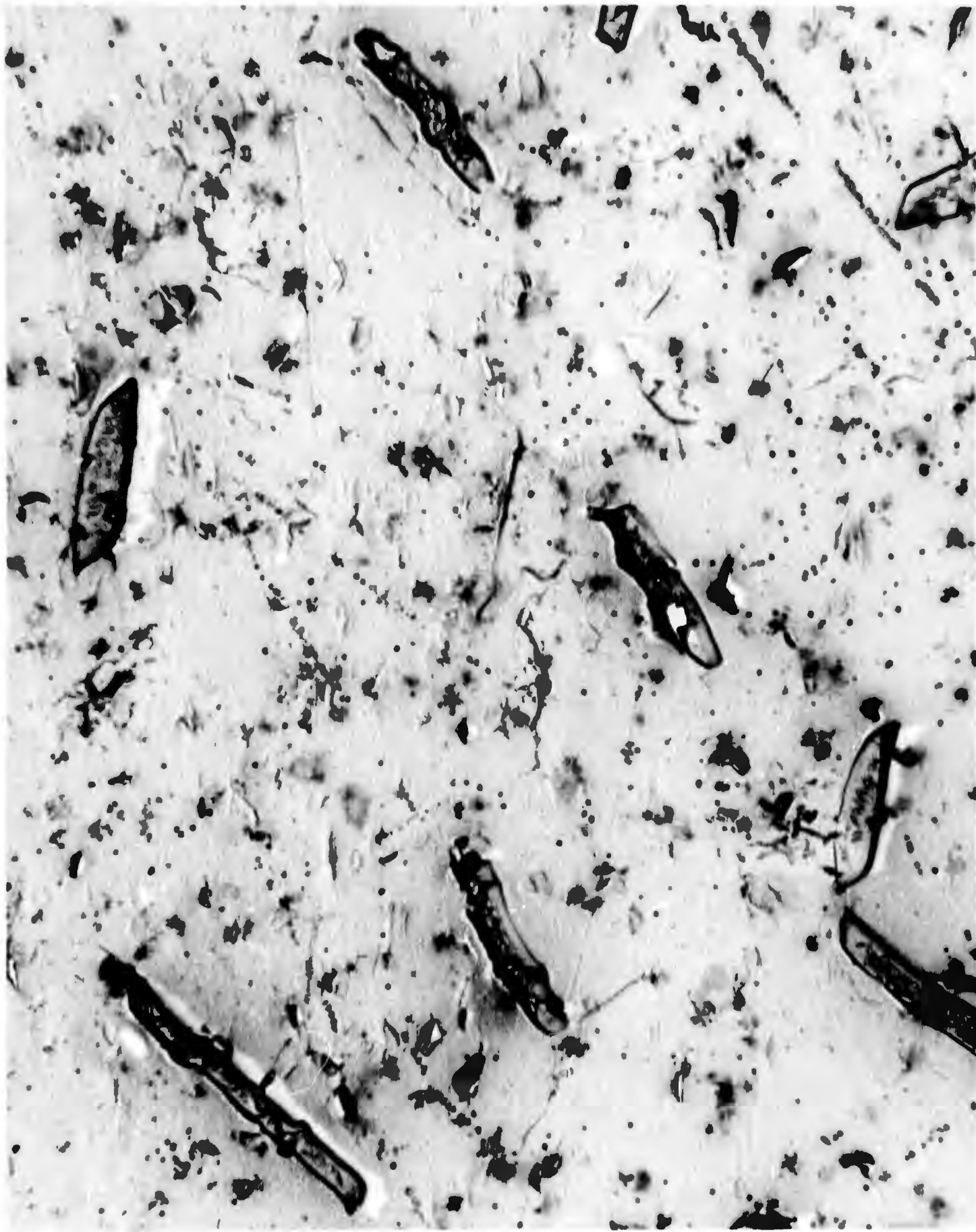


Figure 35. AR-213 Aged at 1200<sup>o</sup> F - Primary CoAl  
in Matrix

The precipitate or decomposition occurring in the primary CoAl at this low aging temperature is unexplained. This is the first stage in the change in morphology of the CoAl.

Magnification: 5000 X

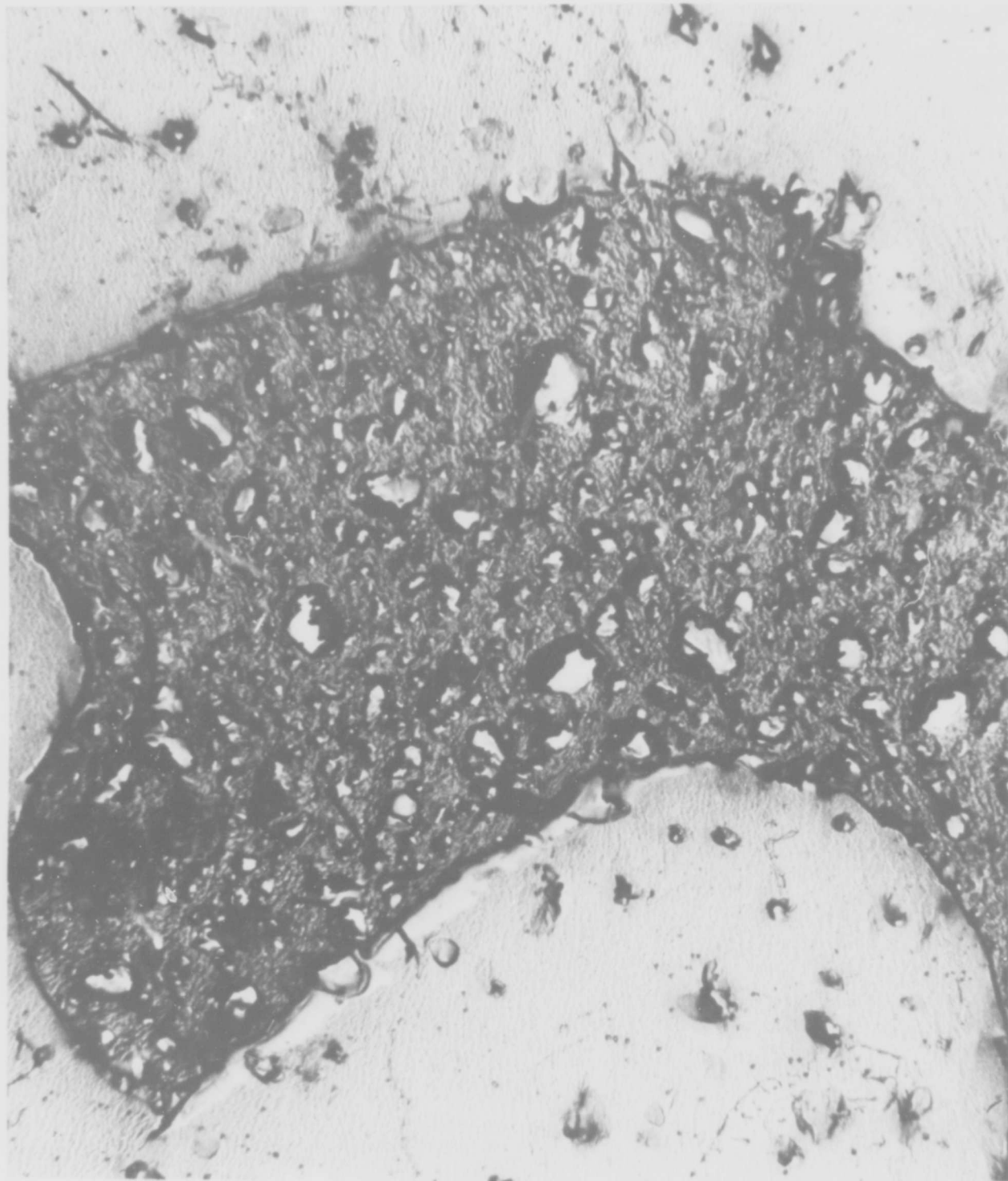


Figure 36. AR-213 Aged at 1400° F - Primary CoAl

This structure shows the next change in decomposition of the CoAl due to a higher aging temperature.

Magnification: 5000 X



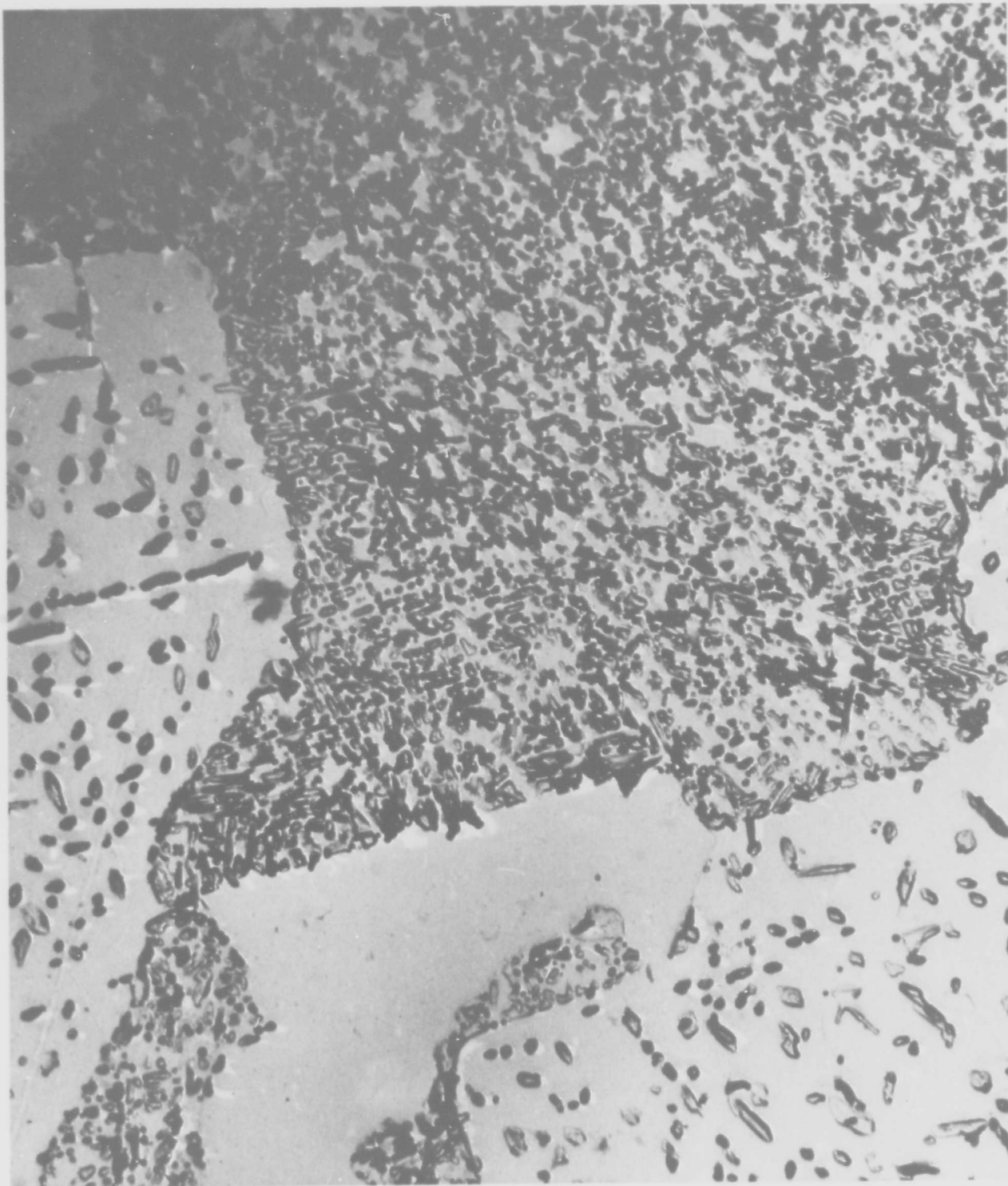


Figure 37. AR-213 Aged at 1400<sup>o</sup> F - Primary CoAl

This is a more highly magnified view of the preceding figure. Note that the texture of the background within the decomposing CoAl is the same as that of the matrix.

Magnification: 10,000 X

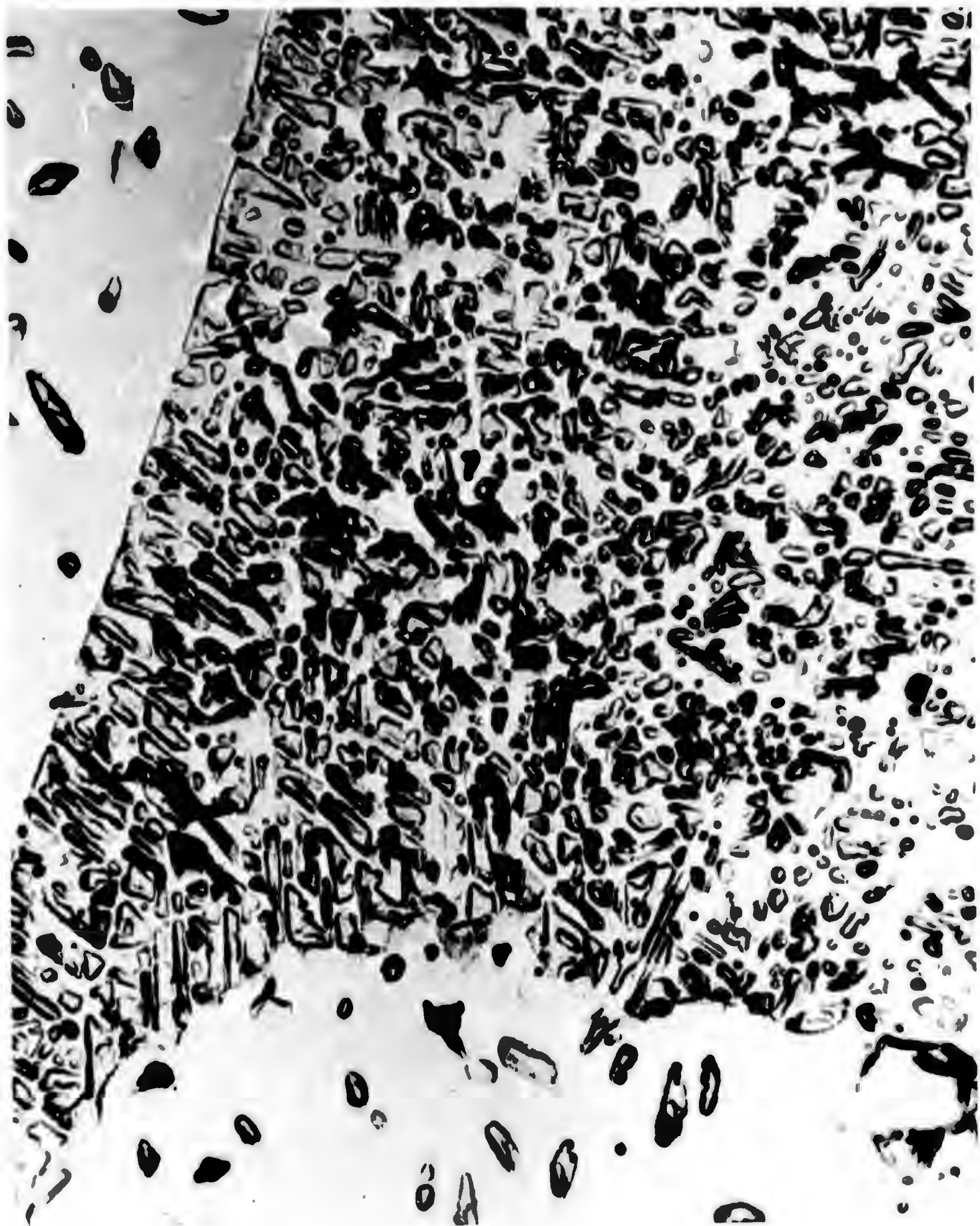


Figure 38. AR-213 Aged at 1400° F - Primary and Secondary CoAl

This microstructure corresponds to the condition of peak hardness for the alloy. The precipitate alignment along definite crystallographic planes is evident. The large primary CoAl phase is undergoing decomposition.

Magnification: 5000 X

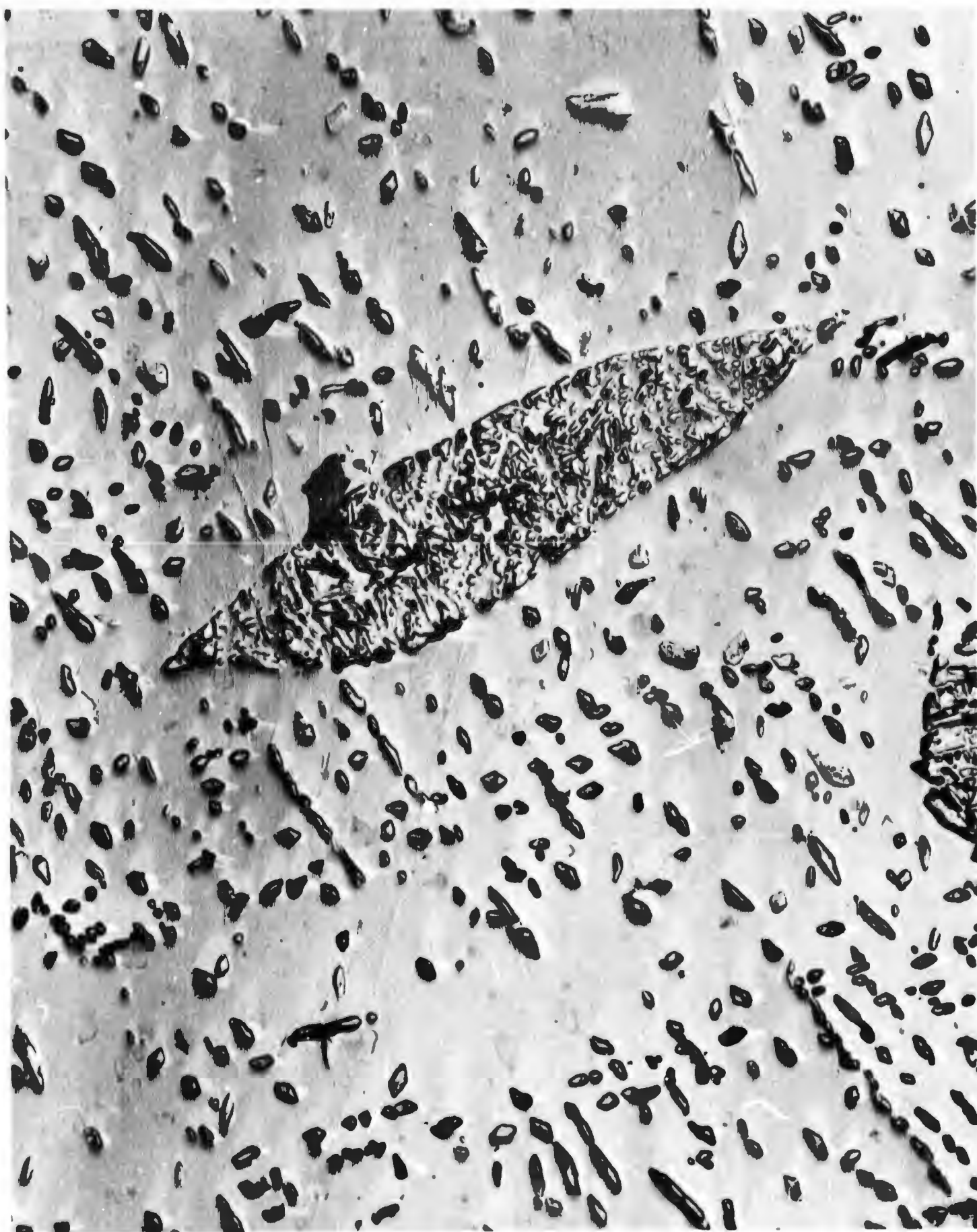


Figure 39. AR-213 Aged at 1400<sup>o</sup> F - Primary CoAl

The structure here is similar to that in Figure 37. The interface between the matrix and CoAl shows the decomposition of the CoAl very clearly.

Magnification: 10,000 X





Figure 40. AR-213 Aged at 1600° F - Primary and  
Secondary CoAl

This not-too-typical structure shows a region where  
the CoAl has almost dissolved in the matrix.

Magnification: 5000 X



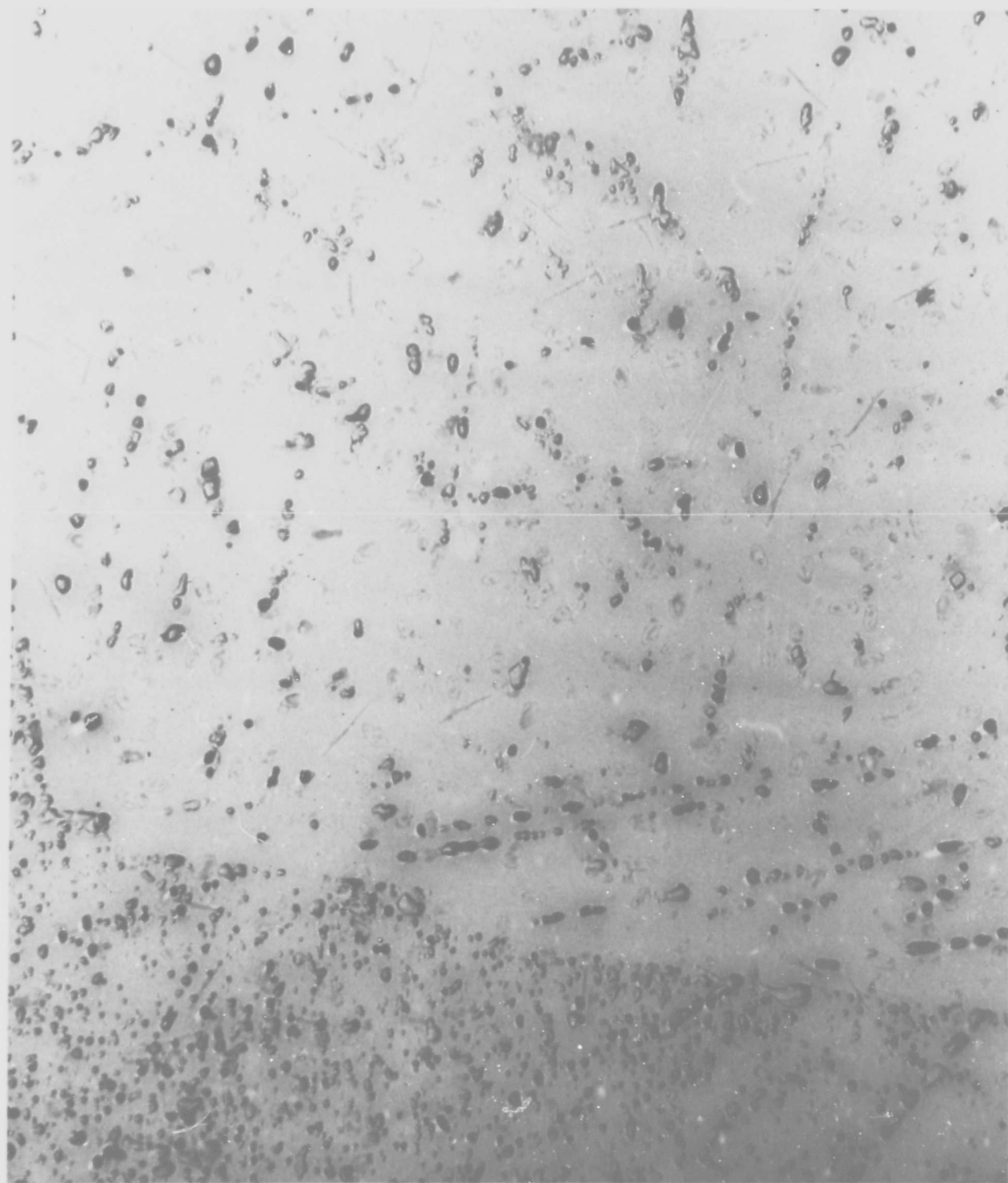


Figure 41. AR-213 Aged at 1600° F - Carbonitride  
in Matrix

The second phase in this structure is that of the  
carbonitride in the matrix.

Magnification: 5000 X



Figure 42. AR-213 Aged at 1700° F - General Matrix

This structure shows the coalesced precipitate at a higher temperature. Their morphology is shown by this view in which both the end-on and top views are visible.

Magnification: 5000 X

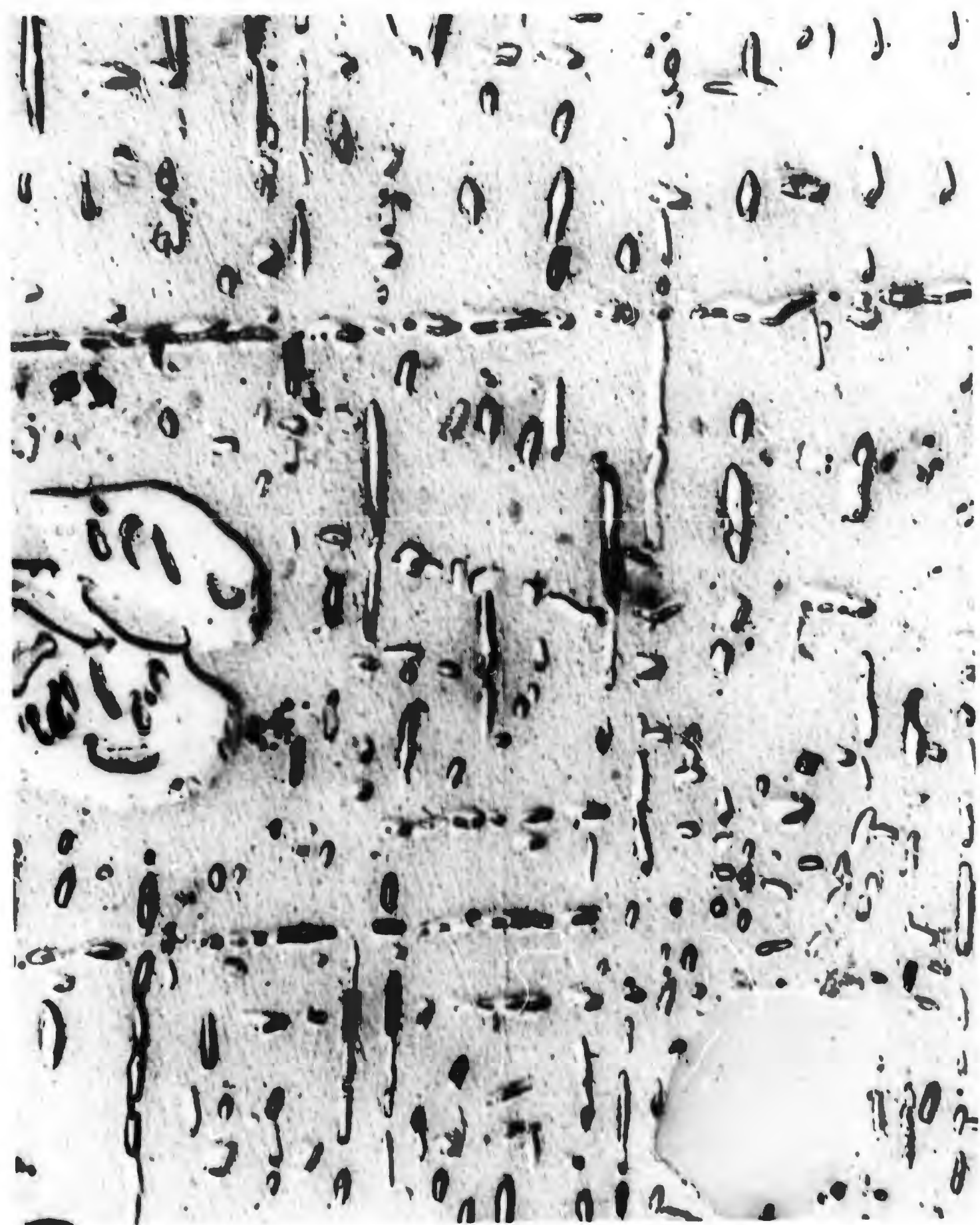


Figure 43. AR-213 Aged at 1700<sup>0</sup> F - General Matrix

This structure, as did that of Figure 42, shows the agglomeration of precipitate in the matrix.

Magnification: 5000 X



Figure 44. AR-213 Aged at 1700<sup>o</sup> F - CoAl  
Decomposition

The decomposition of the CoAl phase at the higher temperatures is by a somewhat different mechanism. The light continuous phase in the center is CoAl. Precipitated in the CoAl is Co solid solution. Note the similarity in texture between the precipitate and the matrix.

Magnification: 5000 X



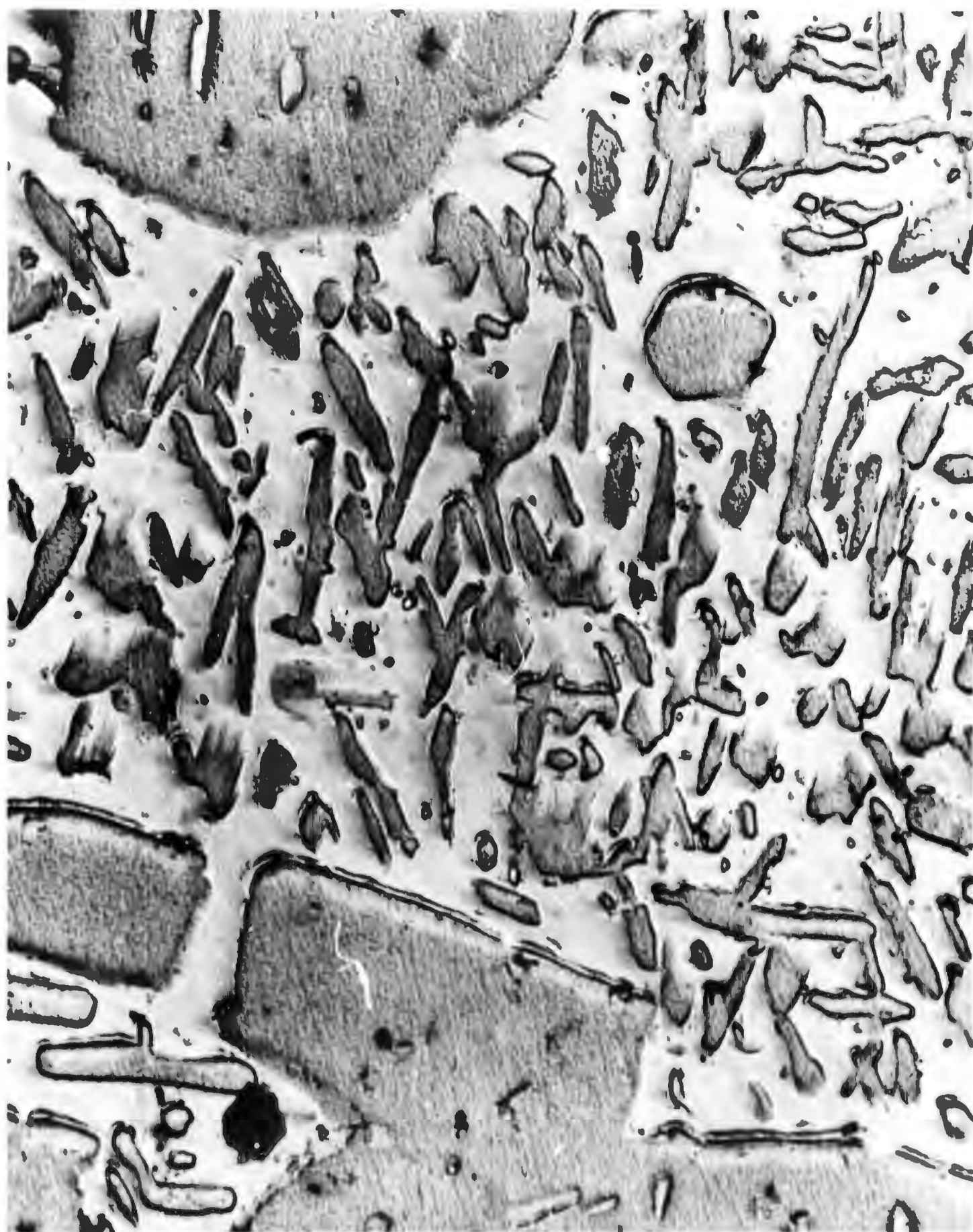


Figure 45. AR-213 Aged at 1800<sup>o</sup> F - General Matrix

The second phase is agglomerated CoAl in the matrix.  
The black areas are artifacts on the replica.

Magnification: 5000 X



Figure 46. AR-213 Aged at 1800<sup>o</sup> F - CoAl  
Decomposition

Precipitation of Co solid solution within the  
primary CoAl phase. Again, the black areas are  
artifacts in the replica.

Magnification: 10,000 X



Figure 47. AR-213 Aged at 1200° F - General Matrix

Agglomerated precipitate in the matrix. It is also suspected that some of the CoAl has started to go back into solution at this temperature.

Magnification: 5000 X





Figure 48. AR-213 Aged at 1900° F - CoAl  
Decomposition

Precipitated Co solid solution within primary CoAl.

Magnification: 10,000 X



